

Tracing ice loss from the Late Holocene to the future in Eastern Nuussuaq, Central-Western Greenland

Josep Bonsoms ^{1*}, Marc Oliva ¹, Juan Ignacio López-Moreno ², Guillaume Jouvét ³

^{1*} Department of Geography, Universitat de Barcelona, Spain.

Email address: josepbonsoms5@ub.edu

² Instituto Pirenaico de Ecología (IPE-CSIC), Campus de Aula Dei, Zaragoza, Spain.

³ Institute of Earth Surface Dynamics, University of Lausanne, Lausanne, Switzerland.

Greenland's peripheral glaciers and ice caps (GICs) have experienced accelerated mass loss since the 1990s. However, the extent to which projected future trends of GICs are unprecedented within the Holocene is poorly understood. This study bridges the gap between the maximum ice extent (MIE) of the Late Holocene, present and future glacier evolution until 2100 in Eastern Nuussuaq Peninsula (Central-Western Greenland). The Instructed Glacier Model (IGM) is calibrated and validated by simulating present-day glacier area and ice thickness. The model is employed to reconstruct the Eastern Nuussuaq Peninsula GICs to align with the MIE of the Late Holocene, which occurred during the late Medieval Warm Period (1130 ± 40 and 925 ± 80 CE), based on moraine boulder surface exposure dating from previous studies. Subsequently, the model is forced with CMIP6 projections for SSP2-4.5 and SSP5-8.5 scenarios (2020-2100). The Late Holocene MIE is reached when temperatures decrease by $\leq 1^\circ\text{C}$ relative to the baseline climate (1960-1990), using a calibrated melt rate factor. Currently, the glaciated area and ice thickness have declined by $15 \pm 5\%$ compared to the MIE, with the standard deviation (\pm) reflecting the influence of the calibrated and low-end melt rate factors. By 2100, temperatures are projected to rise by up to 6°C (SSP5-8.5) above the baseline, exceeding Holocene Warm Period levels (~ 10 to 6 ka) by a factor of three. Ice loss is expected to accelerate rapidly, reaching $-56 \pm 6\%$ relative to present-day levels by 2070-2080 (SSP5-8.5), with near-total glacier disappearance projected by 2090-2100. This study contextualizes present and future glacier retreat within a geologic timescale and quantifies the impacts of anthropogenic climate change on the cryosphere.

Key words: Climate change, glaciology, glacial geomorphology, numerical modelling, deglaciation, Greenland, Arctic.

1. Introduction

Arctic temperatures are rising at a faster (~ 4 times) rate than the global average (IPCC, 2019) and glaciers are displaying accelerated ice loss (Hugonnet et al., 2021). In 2021, Greenland's peripheral glaciers and ice caps (GICs) represented a small (4%) ice cover area of the island but contributed to 11% of the total Greenland ice loss and sea level rise (Khan et al., 2022). The recession of glaciers implies alterations in fauna and flora patterns (Saros et al., 2019), as well as impacts on water availability, climate, and ocean

and atmospheric dynamics that have environmental and climate consequences far beyond the polar regions (IPCC, 2022).

The Little Ice Age (LIA; 1300-1900 CE) has been defined as the last period with widespread glacier expansion (Kjær et al., 2022). Greenland GICs have lost 499 Gt of ice from end of LIA to 2021 (Carrivick et al., 2023). The rate of loss of GICs has increased since the 1990s (Bölch et al., 2013; Larocca et al., 2023), with recent trends indicating an acceleration in mass loss from 27.2 ± 6.2 Gt/yr (February 2003–October 2009) to 42.3 ± 6.2 Gt/yr (October 2018–December 2021) (Khan et al., 2022). Warming rates have been higher in West Greenland than in the East since the end of the LIA (Hanna et al., 2012). As a result, the loss of ice from Greenland's GICs has been more pronounced in its western fringe, where warmer conditions have been associated with the positive phase of the North Atlantic Oscillation (NAO), resulting in a West-to-East warming gradient (Bjørk et al., 2018). Historical records reveal varying trends in GICs over the past two centuries. Aerial images and satellite data indicate that GICs in the West Greenland remained relatively stable, maintaining their extent from the mid-19th century until the mid-20th century, after which they experienced rapid retreat (Weidick, 1994; Leclerq et al., 2012). For instance, Citterio et al. (2009) observed a reduction in glacier area of approximately 20% from the LIA to 2001. Other estimates suggest a 48% loss in GICs area in Southern-Western Greenland since the maximum extent of LIA up to 2019 (Brooks et al., 2022).

The recent evolution of the GICs has been reconstructed using historical aerial images and satellite records (Leclerq et al., 2012; Yde and Knudsen, 2007; Citterio et al., 2009; Bjørk et al., 2018; Larocca et al., 2023). Geospatial techniques, such as the inference of the Equilibrium Line Altitude (ELA), have also been utilized (Brooks et al., 2022; Carrivick et al., 2023). However, aerial and satellite images provide temporal data over centuries and decades and geospatial methods neglect ice-flow physics and do not account for glacier dynamics. Based on the distribution of moraines and unvegetated trimlines in Central-Western Greenland, some authors suggested that the Late Holocene maximum glacier extent occurred around the LIA (Humlum, 1999). However, cosmic ray exposure (CRE) dating of erosive and depositional glacial records indicates that the maximum ice extent (MIE) of the Late Holocene did not occur during the LIA in many areas in Western Greenland but during the Medieval Warm Period (MWP; 950 to 1250 CE) (Young et al., 2015; Jomelli et al., 2016; Schweinsberg et al., 2019).

Compared to studies near the GrIS (e.g., Cuzzzone et al., 2019; Briner et al., 2020), there is limited evidence from physically-based models regarding the GIC recession during the Holocene. . Holocene reconstructions of GrIS extent based on physical modelling, guided by geomorphological evidence, provide valuable insights into the paleoclimate conditions that led to the MIE of the Late Holocene and subsequent recession (Simpson et al., 2009; Lecavalier et al., 2014; Cuzzzone et al., 2019), facilitating comparisons of past and future glacier responses to climate change (Briner et al., 2020). Physical-based ice-flow modelling relying on full-Stokes equations are computationally intensive at high resolution (sub-kilometer) for long-term paleo glacier simulations and model parameter

calibrations (Jouvet et al., 2022). Simplified models such as the hydrostatic Shallow Ice Approximation (SIA) and the Shallow Shelf Approximation (SSA) tend to overestimate ice velocities near glacier margins and underestimates velocities in deep glaciated areas, respectively. An emulator based on a convolutional neural network (CNN), trained with high-order ice flow equations, offers reduced computational costs while maintaining accurate ice thickness estimates comparable to those obtained through high-order equations (Jouvet, 2023a; 2023b).

The future recession of Greenland GICs compared to the long-term Holocene fluctuations is poorly understood. Here, we calibrate and validate the Instructed Glacier Model (IGM) (Jouvet et al., 2023a), a glacier evolution model based on a CNN emulator to estimate ice flow, to reconstruct the MIE of the Late Holocene in an extended glacier area in the Eastern Nuussuaq Peninsula (Central-Western Greenland). This area has CRE records available for the outermost glacier moraine complexes but the paleoclimate conditions causing these glacier oscillations are not yet known in detail (D'andrea et al., 2011; Biette et al., 2019; Jomelli et al., 2016; Schweinsberg et al., 2019; Osman et al., 2021). Employing IGM allows us to reconstruct glaciers in high (90 m) resolution based on high-order equations (Jouvet, 2023a), demonstrating the methodology's capabilities for glacier modeling at regional scales. Future glacier evolution is modeled under the CMIP6 SSP2-4.5 and SSP5-8.5 scenarios, from present and steady-state glacier conditions to the year 2100. We compared the projected ice loss trend against the reconstructed MIE of the Late Holocene to the present-day ice loss trends, extending glacier records from decades to millennia and placing present and future glacier shrinkage within a long-term Holocene perspective.

The objectives of this work are to (i) reconstruct past glaciers under different climate conditions, (ii) determine past and future climate conditions influencing the MIE of the Late Holocene and future glacier recession, (iii) quantify future glacier retreat trends, and (iv) compare future ice loss trends with the rate of ice loss from the MIE of the Late Holocene to the present.

2. Study area

This study focuses on a land-terminating glacier area in the Nuussuaq Peninsula, Central-West Greenland (Figure 1). This peninsula extends from the onshore Disko (South) to Svartenhuk Halvo (North). Nuussuaq Peninsula includes several mountain glaciers and ice caps connected to the GrIS that surrounds its Eastern flank. Our study focuses on a glacier area in the Eastern Nuussuaq Peninsula, with elevations ranging from 400 to 1200 meters above sea level (m a.s.l.) (Figure 1).

Present-day climate conditions are characterized by a polar maritime climate, becoming more continental toward the inland areas and GrIS (Humlum, 1999). Moist air masses from the Davis Strait influence the climate during summer, with continental polar air influences during the winter (Ingolfsson et al., 1990). Prevailing winds in the region typically come from the East and North-East, except during the summer months, when

Southerly and Southern-Western winds prevail (Humlum, 1999). The relief configuration exposes Disko Bugt to cyclogenetic activity and moist airflow, resulting in decreased precipitation from the peripheral coastal areas towards the GrIS (Weidick and Bennike, 2007). The nearest research station with meteorological and snow observations is the Arctic station, at coastal Disko Island (Central-Western Greenland). Here, the accumulated annual precipitation is 436 mm (1991–2004 period) (Hansen et al., 2006). The mean annual temperature (MAAT) is -4°C (1961–1990 period), with a lapse rate of around 0.6°C per 100 m (Humlum, 1998). At Arctic station, the snow season typically extends from September to June, with maximum snow accumulations of around 50 cm (Bonsoms et al., 2024).

The present-day landscape in Central-West Greenland is characterized by the presence of glaciers, which have also intensely shaped the relief in ice-free areas in the past. Today, environmental dynamics in these areas is strongly influenced by periglacial processes under a continuous permafrost regime (Humlum, 1998; Christiansen et al., 2010) that reshape the geological setting made of clastic sediments from the Mid-Cretaceous to the Palaeogene (Pedersen et al., 2002). The strong glacial imprint in the landscape of the peninsula results from a complex glacial history, which is not yet known in detail. Following the LGM, the GrIS underwent a significant retreat during Termination-1 and exposed the coastal regions in Central-West Greenland (Briner et al., 2020). As in other regions across Greenland, the Early Holocene was characterized by warm temperatures that led glaciers to retreat (Leger et al., 2024). In the Nuussuaq Peninsula, CRE records reported the onset of glacial retreat by ca. 10 ka (O’Hara et al., 2017). The minimum GrIS extension occurred from ca. 5 to 3 ka cal BP, when GrIS margins retreated by ca. 150 km from present-day terminus position (Briner et al., 2016), which explains the lack of glacial records corresponding to the Early-Mid Holocene in the peninsula (Kelly and Lowell, 2009; O’Hara et al., 2017). According to several absolute dating methods in different natural records, the Nuussuaq Peninsula GICs grew between approximately 4.3 and 2 ka and reached several glacier culminations during the past millennium before the LIA (Schweinsberg et al., 2017; 2019). The internal and external moraine complexes in the area reported CRE ages of 1130 ± 40 and 925 ± 80 CE, respectively (Young et al., 2015). These ages are consistent with other CRE ages obtained in Central-Western Greenland for the most external recent moraine complexes, indicating that the late MWP glacier expansion was the largest of the Late Holocene (Jomelli et al., 2016; Schweinsberg et al., 2019).

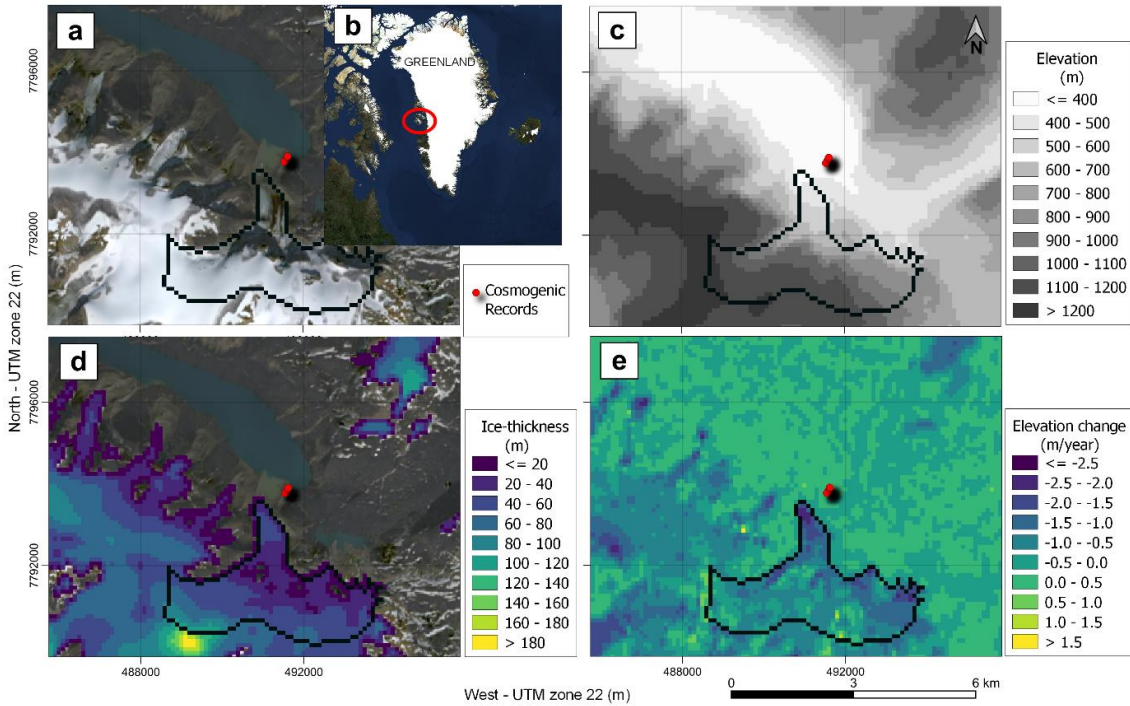


Figure 1. Location of the reconstructed glacier and CRE ages (red points) used in this work (a). Location of the study area within Greenland (b). Glacier delimitation is based on Randolph Glacier Inventory (RGI6). The base map is a Sentinel-2 image from <https://s2maps.eu/> (2022). Elevation map of the study area from a Digital Elevation Model Copernicus DEM GLO-90 (2010-2015) (c). Average ice thickness (m) (2018-2022) from Millan et al. (2022) (d). Elevation changes average values (m/year) between 2000-2019 (Hugonnet et al., 2021) (e).

3. Data

3.1 Pre-processing glacier data downloading

The data used to force and validate the IGM is detailed at Table 1. Topography data were obtained from a Copernicus Digital Elevation Model (DEM) with a resolution of 90 meters (COPERNICUS DEM GLO-90). In-situ mass balance records in the study area are scarce and fieldwork is challenging. However, recent advancements in global-scale mass balance, satellite imagery, and ice thickness estimates have enabled the validation of the glacier model. We compared the ice thickness estimates from Farinotti et al. (2019), which are the output from an ensemble of five models (HF-model, GlabTop2, OGGM, GlabTop2 IITB version, and an unnamed model), with those from Millan et al. (2022), which are derived from numerical modeling based on SIA and data obtained from a constellation of remote sensing products (Sentinel-1/ESA, Sentinel-2/ESA, Landsat-8/USGS, Venus/CNES-ISA, Pléiades/Airbus D&S). Glacier mask outlines were acquired from the Randolph Glacier Inventory Version 6 (RGI6.0). Elevation change rate (dh/dt) data were obtained from Hugonnet et al. (2021).

The climate variables required to run the IGM model are monthly accumulated precipitation ($\text{kg m}^{-2} \text{ yr}^{-1}$), monthly average air temperature ($^{\circ}\text{C}$), and monthly air temperature standard deviation ($^{\circ}\text{C}$) from the nearest pixel to the glacier. We utilized the GSWP3 W5E5v2 monthly dataset at a spatial resolution of $0.5^{\circ} \times 0.5^{\circ}$, which combines the Global Soil Wetness Project phase 3 dataset with the bias-adjusted ERA5 reanalysis dataset (Cucchi et al., 2020). Future glacier changes are modeled based on bias-corrected monthly accumulated precipitation and monthly average air temperature CMIP6 multi-model mean ($n=33$) for SSP2-4.5 and SSP5-8.5 (2020 to 2100) at a spatial resolution of 0.25° (Thrasher et al., 2022), subtracted at the nearest grid point of the glacier with cosmogenic exposure nuclide data. Months are aggregated into seasons as follows: September, October, November (Autumn), March, April and May (Spring), December, January and February (Winter), June, July and August (Summer). Data were downloaded using Open Global Glacier Model (OGGM) model (<https://oggm.org/>) (Maussion et al., 2015) module of IGM (Jouvet et al., 2023a), except for CMIP6 projections (Thrasher et al., 2022) and ice thickness estimates (Farinotti et al., 2019).

Table 1. Characteristics of the datasets employed for forcing, calibrating, and validating the IGM.

Description	Name	Spatial resolution	Database Date	Source
DEM	Copernicus DEM GLO-90	90 m	2010-2015	https://spacedata.copernicus.eu/documents/20126/0/CSC_DA_ESA_User_Licence_2021_11_17.pdf
Ice-thickness (1)	Millan et al. (2022)	100 m	2017-2018	Millan et al. (2022)
Ice-thickness (2)	Farinotti et al. (2019)	25 m	2019	Farinotti et al. (2019)
Baseline climate data	GSWP3_W5E5v2.0	$0.5^{\circ} \times 0.5^{\circ}$	1960-1990	https://data.isimip.org/search/simulation_round/ISIMIP2a/product/InputData/climate_forcing/gswp3-w5e5/
CMIP6 projections	CMIP 6	0.25°	1960-2100	Thrasher et al. (2022)
Dh/dt	Hugonnet et al. (2021)	Glacier (RGI6.0) level	2000-2020	Hugonnet et al. (2021)
Glacier Outline	RGI6.0	Glacier (RGI6.0) level	2003	https://www.glims.org/RGI/

3.2 Geomorphological and paleoclimate data

The CRE ages are based on nuclide (^{10}Be) introduced by Young et al. (2015) and refer to the period of the maximum glacier advance of the last warm/cold cycles in the Nuussuaq Peninsula and were used for the paleoclimate modelling purposes of this study. The sampled boulders were obtained from the outer ridge of the moraine and reveal either (i) a period of glacial surge or (ii) a phase of stabilization/stillness during the long-term retreat. However, special caution must be taken when interpreting these ages, as they are not directly indicative of the period of ice occupation but of the timing of stabilization of moraine boulders.

Paleoclimate anomalies with respect to the baseline climate were obtained from annual air temperature reconstructions from ice cores of the GrIS and margins of the GrIS provided by Buizert et al. (2018). This data ranges from the Last Glacial Maximum (LGM; $\sim 26\text{-}19$ ka ago) to 2000 CE.

4. Methods

4.1 Instructed Glacier Model (IGM)

The IGM is a glacier model that simulates ice thickness evolution according to ice mass conservation principles, surface mass balance and ice flow physics (Jouvet et al., 2023a). IGM updates the ice thickness at each time step from ice flow and surface mass balance (SMB) by solving the mass conservation equation. The ice flow is modelled using a CNN model that is trained to satisfy high-order ice flow equations. The strength of the ice flow is modeled through the rate factor (A) that controls the ice viscosity in Glen's flow law (Glen, 1955), expressed as:

$$\dot{D} = A\tau^n,$$

Where \dot{D} and τ are the strain rate and deviatoric stress tensors, respectively and n is Glen's exponent, 3 (Glen, 1955). The basal sliding is modeled using the nonlinear sliding law of Weertman (Weertman, 1957), expressed as:

$$u_b = c \tau_b^{1/m},$$

Where u_b is the sliding velocity, c is the basal sliding, τ_b is the basal shear stress, and m is a constant of 1/3. The parameters A and c are parametrized (c.f. section 4.2) to reproduce available ice thickness datasets (Farinotti et al., 2019; Millan et al., 2022).

The IGM implements SMB estimation based on a recent state-of-the-art calibration introduced by Marzeion et al. (2012) and implemented in OGGM v1.6.1 by Maussion et al. (2019). Precipitation is extrapolated across the DEM area, while temperature data are downscaled using a reference height and a constant lapse rate of $-0.65^\circ\text{C}/100$ m, consistent with annual lapse rates reported in the literature, such as $0.65^\circ\text{C}/100$ m at low elevations of the GrIS (Hanna et al., 2005) and Disko Island (Humlum, 1998). This value is similar to the average lapse rate during the pre-industrial period and early Holocene ($0.7^\circ\text{C}/100$ m; Erokhin et al., 2017). Additionally, a sensitivity analysis was performed to assess the impact of the temperature lapse rate on ice-thickness anomalies in the

reconstruction. The analysis compared results using a lower lapse rate ($0.55^{\circ}\text{C}/\text{m}$), the applied lapse rate ($0.65^{\circ}\text{C}/\text{m}$), and a higher lapse rate ($0.75^{\circ}\text{C}/\text{m}$). The OGGM v1.6.1 calibration corrects climate data to avoid systematic biases, including the effects of avalanches, relief shadowing, negative precipitation biases, and topographical shading. This correction is applied using a multiplicative factor calibrated to match geodetic mass balance data for the 2000–2020 period from Hugonnet et al. (2021). Precipitation is classified as solid ($< 0^{\circ}\text{C}$) or liquid ($> 2^{\circ}\text{C}$), with a linear transition between solid and liquid phases. The melting threshold is set at -1°C , and the density of water is fixed at $1000 \text{ kg}/\text{m}^3$. SMB is estimated using a monthly positive degree-day (PDD) model (Hock, 2003; Huss, 2008). The PDD is calibrated based on a melt factor (5, in this case) to match the glacier geodetic mass balance of Hugonnet et al. (2021) for the 2000–2020 period. The melt rate factor is adjusted to estimate uncertainties in past and future conditions by applying low- and high-end melt rates (cf. Sections 4.2 and 4.3). This calibration aligns with recent GICs calibrations, as detailed in Marzeion et al. (2012), Aguayo et al. (2023), and Zekollari et al. (2024). Further details on the OGGM v1.6.1 SMB calibration process are provided in the OGGM documentation (<https://docs.oggm.org/en/v1.1/mass-balance.html#calibration>). The physical basis of IGM is described in Jouvett et al. (2022, 2023a) and references therein. The model and its physical framework are available at <https://github.com/jouvetg/igm>.

4.2 Present day glacier calibration and validation

The IGM is calibrated to simulate the RGI6.0 area and ice thickness using available datasets (Farinotti et al., 2019; Millan et al., 2022). The IGM parametrization was performed by conducting a sensitivity analysis to spin-up temperature and ice-flow dynamics, adjusting the parameters A and c . These parameters were selected to optimize the IGM and accurately simulate various ice conditions, basal sliding conditions, and subglacial hydrology. A set of parameter options ($n = 36$) was tested over a 1000-year model run to achieve long-term (> 500 years) glacier area steady-state conditions and reproduce the RGI6.0 area and ice thickness from the available datasets (Farinotti et al., 2019; Millan et al., 2022). The calibration parameter options include different temperature perturbations. For a calibrated melt rate factor (see Section 4.1), temperature perturbations of -0.75°C , -0.5°C , 0°C , and $+0.25^{\circ}\text{C}$ are applied relative to the baseline climate (1960–1990). For a low-end melt rate factor (3), temperature perturbations range from 0.75°C to 1.25°C in increments of 0.25°C . For a high-end melt rate factor (9), temperature perturbations range from -1.75°C to -1.25°C in increments of 0.25°C . The range of temperature perturbations was determined through trial and error, which showed that values outside this range produced higher discrepancies compared to the available datasets used for validation (Figures 3, 5, S1 and S2). Regarding ice-flow dynamics, a sensitivity analysis was performed on IGM parametrization to simulate cold, temperate, and soft ice conditions by changing A from $34 \text{ MPa}^{-3} \text{ a}^{-1}$, $78 \text{ MPa}^{-3} \text{ a}^{-1}$ (IGM default value) to $150 \text{ MPa}^{-3} \text{ a}^{-1}$. Basal sliding conditions are parametrized by changing c from $0.01 \text{ km MPa}^{-3} \text{ a}^{-1}$, $0.03 \text{ km MPa}^{-3} \text{ a}^{-1}$ (IGM default value), and $0.05 \text{ km MPa}^{-3} \text{ a}^{-1}$. The IGM parameterization is shown in Figures 3 to 5. An analysis of the influence of the IGM

calibrated ice-dynamics options and the default configuration is also performed. All other parameters were kept at their default IGM configuration.

The accuracy evaluation of the modeled IGM outputs is based on both area and ice thickness. We calculated (i) the Mean Absolute Error (MAE) between the accumulated glacier ice thickness from Farinotti et al. (2019) and Millan et al. (2022) and the output from IGM; (ii) the glacier area difference between RGI6.0 area and from IGM. To incorporate both area and ice thickness errors, we calculated the bias by multiplying the ice thickness MAE (i) by the area difference (ii).

4.3 Past and future glacier evolution

To accurately reconstruct the glaciated area, it is necessary to model the region beyond the glacier using CRE data. The IGM is applied to a region of interest in Eastern Nuussuaq, which includes 25 glaciers from the RGI6.0 database and covers a total area of 154 km². The IGM is forced with the lowest error parameterization option and the default IGM configuration until the glaciated area reaches present-day and long-term stable-state conditions. To model past ice thickness, a calibrated melt rate (5) based on mass balance data (2000-2020) is used (see Section 4.1). Additionally, a low-end melt rate (3) is applied, representing the lower (3) and upper (5) bounds of the PDD calibration, to provide confidence intervals for past reconstructions. For reconstructing the glaciated area, the model is run again over 1000 years with an ensemble of different temperature and precipitation values to simulate the MIE of the Late Holocene from the MWP. For the calibrated melt rate factor, the temperature was perturbed over the baseline climate from 0 to -1.5°C in steps of 0.25°C. For the low-end melt rate, the temperature was perturbed over the baseline from 0.75 to 1.25°C in steps of 0.25°C. Precipitation was kept unchanged (0%) and also increased by 10% to estimate whether high rates of snowfall could compensate for warming. The MIE of the Late Holocene paleoclimate conditions were determined by calculating the distance between the glacier tongue of the ensemble of simulations and the CRE dates of the outer ridge moraines (Köse et al., 2022). The simulations that match the outer ridge moraines represent the climate conditions prior to the CRE dates. The present-day glacier area with steady-state conditions is the starting point for future glacier projection simulations (Zekollari et al., 2019). We used a calibrated melt rate (5) and a high-end melt rate (9) to define the lower and upper confidence intervals, respectively. The IGM is run from the present day until 2100 using monthly accumulated precipitation and average air temperature CMIP6 multi-model mean SSP2-4.5 and SSP5-8.5 anomalies relative to the baseline climate, applying additive factors for temperature and multiplicative factors for precipitation (Rounce et al., 2023).

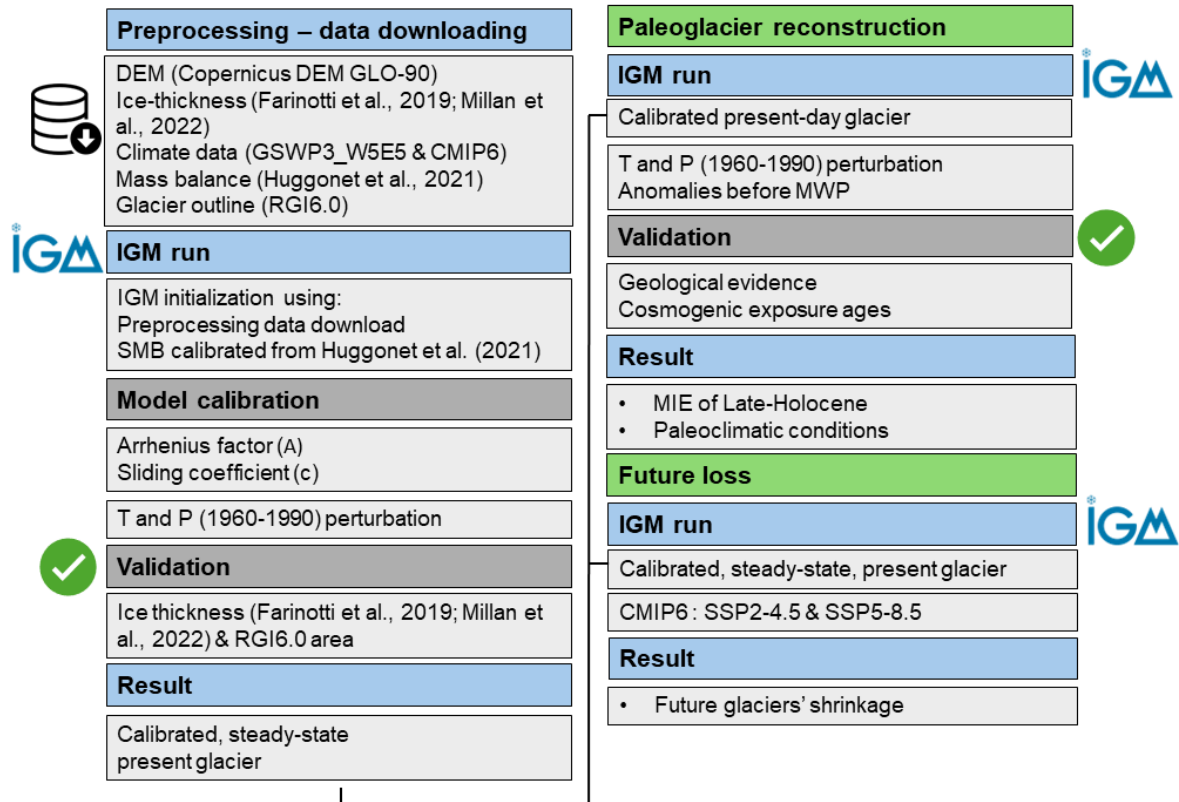


Figure 2. Flowchart followed for reconstructing past and present glaciers and projecting their future evolution based on air temperature (T) and precipitation (P). The symbols next to the graph are included to make it easier to visually associate elements and enhance interpretability within the figure.

5. Results

5.1 IGM parametrization and calibration

For most IGM parametrizations, glacier growth occurred until 350 to 600 years of spin-up. The latest year of the spin-up simulation is subsequently validated against ice thickness estimates (Farinotti et al., 2019; Millan et al., 2022). The error metric values for ice thickness and area resulting from the IGM calibration and parametrization process are shown in Figure 3, 5, S1 and S2. Using a calibrated melt rate factor the most favorable range for achieving accurate results for present-day data is a perturbation range of temperature from 0°C to -0.5°C with respect to the baseline climate (Figure 3 to 5). The largest errors in ice thickness and glacier area were observed for the $A = 34 \text{ MPa}^{-3} \text{ a}^{-1}$ and $c = 0.01 \text{ km MPa}^{-3} \text{ a}^{-1}$ IGM configuration. This configuration tended to overestimate ice thickness for both global-scale ice thickness references (Figure 4 and 5). Additionally, using the default configuration and reducing the temperature to $< -0.5 \text{ °C}$ over the baseline climate led to overestimations of ice thickness.

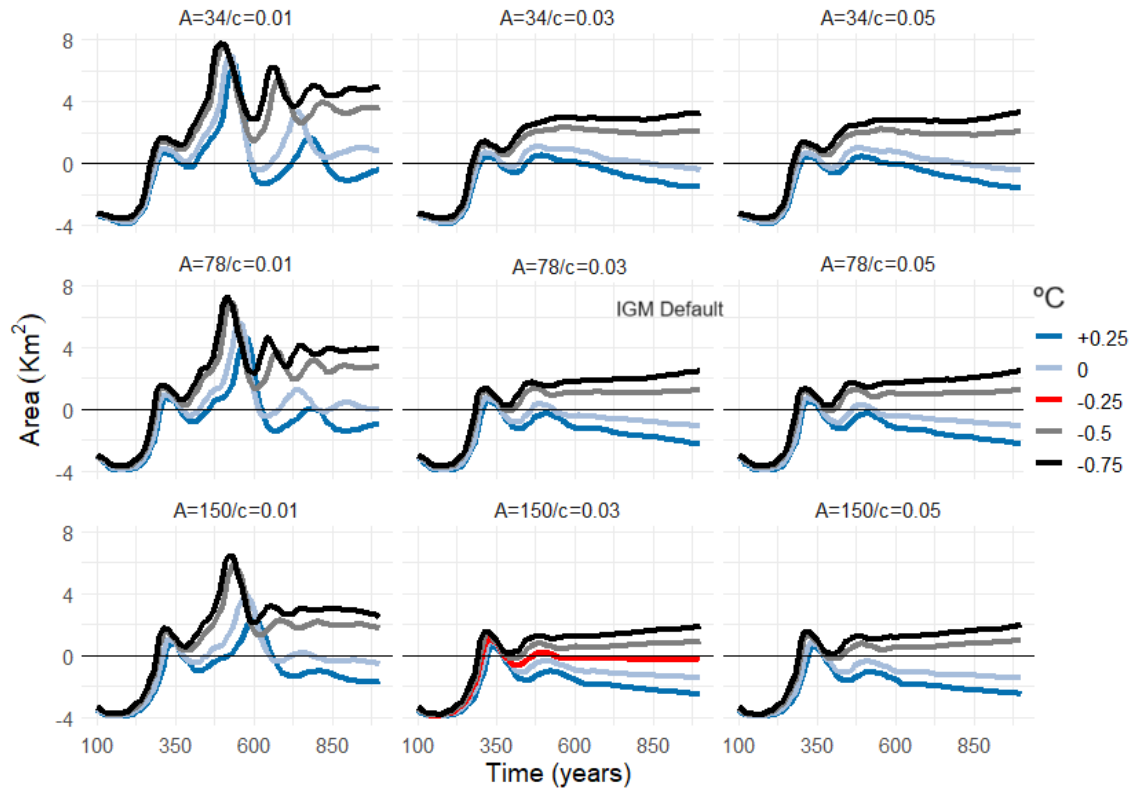


Figure 3. Difference from the RGI6.0 area and IGM outputs within a 1000-years spin-up. Data is grouped by changes in temperature (colors), A and c options (boxes). The selected configuration ($A = 150 \text{ MPa}^{-3} \text{ a}^{-1}$ and $c = 0.03 \text{ km MPa}^{-3} \text{ a}^{-1}$, -0.25°C with respect to the baseline climate) is shown in red color.

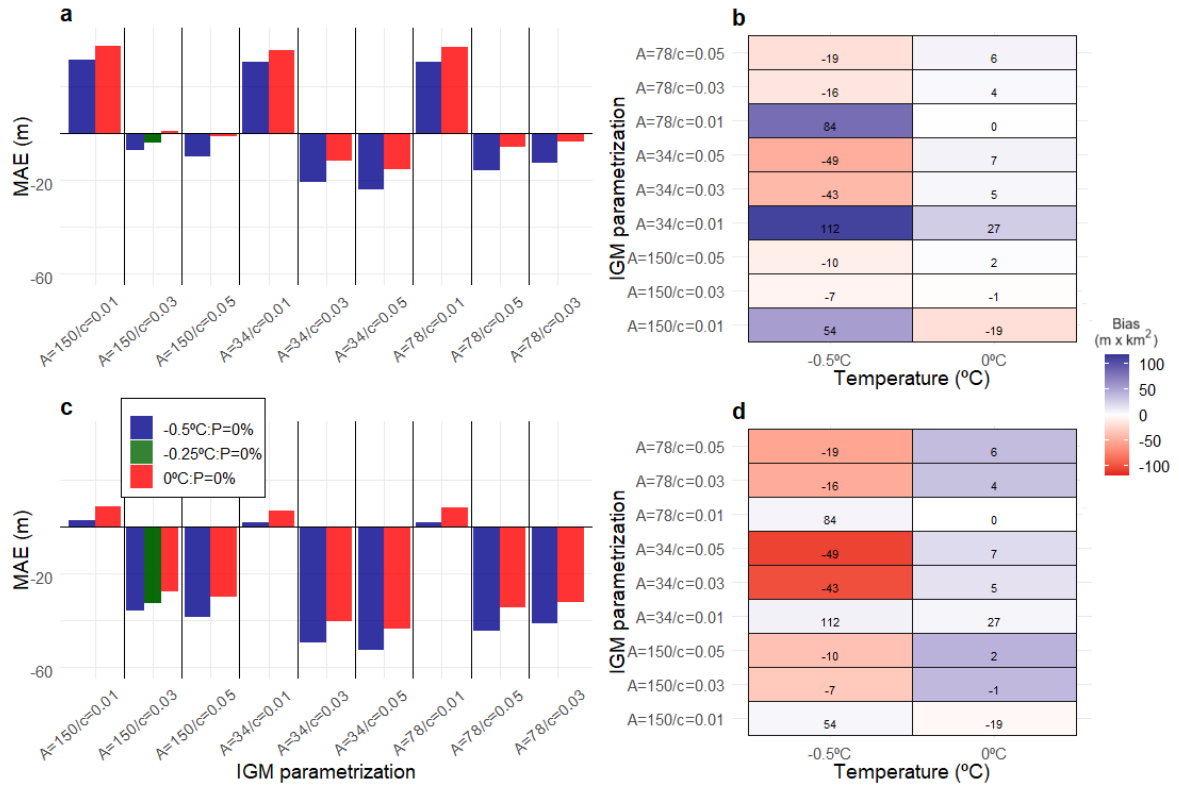


Figure 4. Ice thickness MAE between Farinotti et al. (2019) and IGM outputs after spin-up with different A and c parametrizations and perturbations of temperature (a). The selected configuration is shown with green color. Ice thickness MAE values from Figure 4 (a) multiplied by the difference between the RGI6.0 area and the IGM outputs (bias) for different A and c parametrizations and perturbations of temperature (b). Figure 4 (c) and (d) are the same as Figure 4 (a) and (b), respectively, but for ice thickness estimates from Millan et al. (2022).

Trial and error parametrizations of A and c revealed that optimal results were achieved for $A = 150 \text{ MPa}^{-3} \text{ a}^{-1}$ and $c = 0.03 \text{ km MPa}^{-3} \text{ a}^{-1}$. These outputs of the IGM align with Farinotti et al. (2019). However, both IGM ice thickness and Farinotti et al. (2019) overestimate ice thickness compared to Millan et al. (2022) (Figures 4 and 5). Setting $A = 150 \text{ MPa}^{-3} \text{ a}^{-1}$ and $c = 0.03 \text{ km MPa}^{-3} \text{ a}^{-1}$, with a slight variation of temperature (-0.25°C) over the baseline climate, resulted in very similar accumulated ice thickness to Farinotti et al. (2019) ($\text{MAE} = 4 \text{ m}$; Figure 4a), a minimal RGI6.0 area bias (Figure 3 and 4b), and very stable-state glacier conditions for > 500 years (Figure 3). This configuration also minimized errors against the Millan et al. (2022) dataset ($\text{MAE} = 24 \text{ m}$) (Figure 4c). Glacier reconstruction and projection are based on this parameterization option. Additionally, the default IGM configuration ($A = 78 \text{ MPa}^{-3} \text{ a}^{-1}$ and $c = 0.03 \text{ km MPa}^{-3} \text{ a}^{-1}$), with the temperature perturbation that results in the lowest error, is included in past and future simulations to account for uncertainties in ice-flow dynamics. Past reconstructions and future glaciated area simulations are performed using the calibrated melt rate, as well as low (3) and high (9) melt rates, which define the confidence intervals for past and future projections. These melt rates are calibrated to reproduce present-day

conditions. To achieve this, temperature adjustments relative to the baseline climate were set to +1.25°C for the low melt rate and -1.5°C for the high melt rate (Figures S1 and S2).

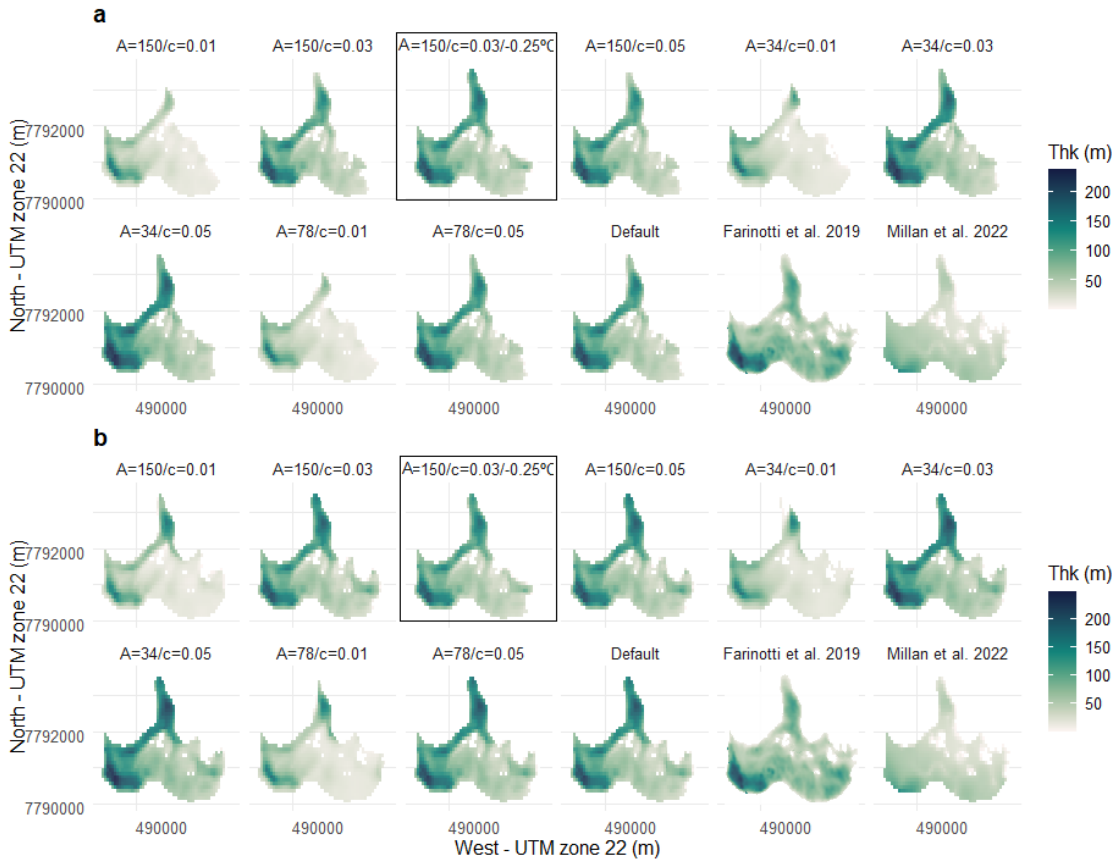


Figure 5. Average ice thickness data from Farinotti et al. (2019) and Millan et al. (2022), along with examples of IGM configuration options using different A and c parameters for the selected configuration (highlighted with a black square), are shown for a temperature of 0°C with respect to the baseline climate (a) and a temperature of -0.5°C with respect to the baseline climate (b). The ice thickness values of IGM shown are the result of steady-state glacier conditions.

5.2 Late Holocene maximum glacier extension and paleoclimatic conditions

The temperature evolution from the LGM to 2000 CE, as reconstructed from GrIS ice cores and Greenland margins (Buizert et al., 2018), is shown in Figure 6. The Camp Century and Disko Bugt/Jakobshavn ice cores exhibit similar temperature trends compared to the baseline climate period, although they display larger temperature anomalies, with the warmest conditions recorded during the Holocene Warm Period (HWP; ~ 9-5 ka ago) (up to 3°C with respect to the baseline climate period). A long-term cooling trend is detected for the Late Holocene, with moderate anomalies and high yearly oscillations of around ± 1 °C between the Dark Ages Cold Period (~ 400 to 765 CE;

Helama et al., 2017) and the MWP for Disko Bugt/Jakobshavn (Figure 6). However, colder temperatures are found in the Camp Century ice core. For both locations, the coldest temperature anomalies of ca. -2°C compared to the baseline climate are found during the LIA.

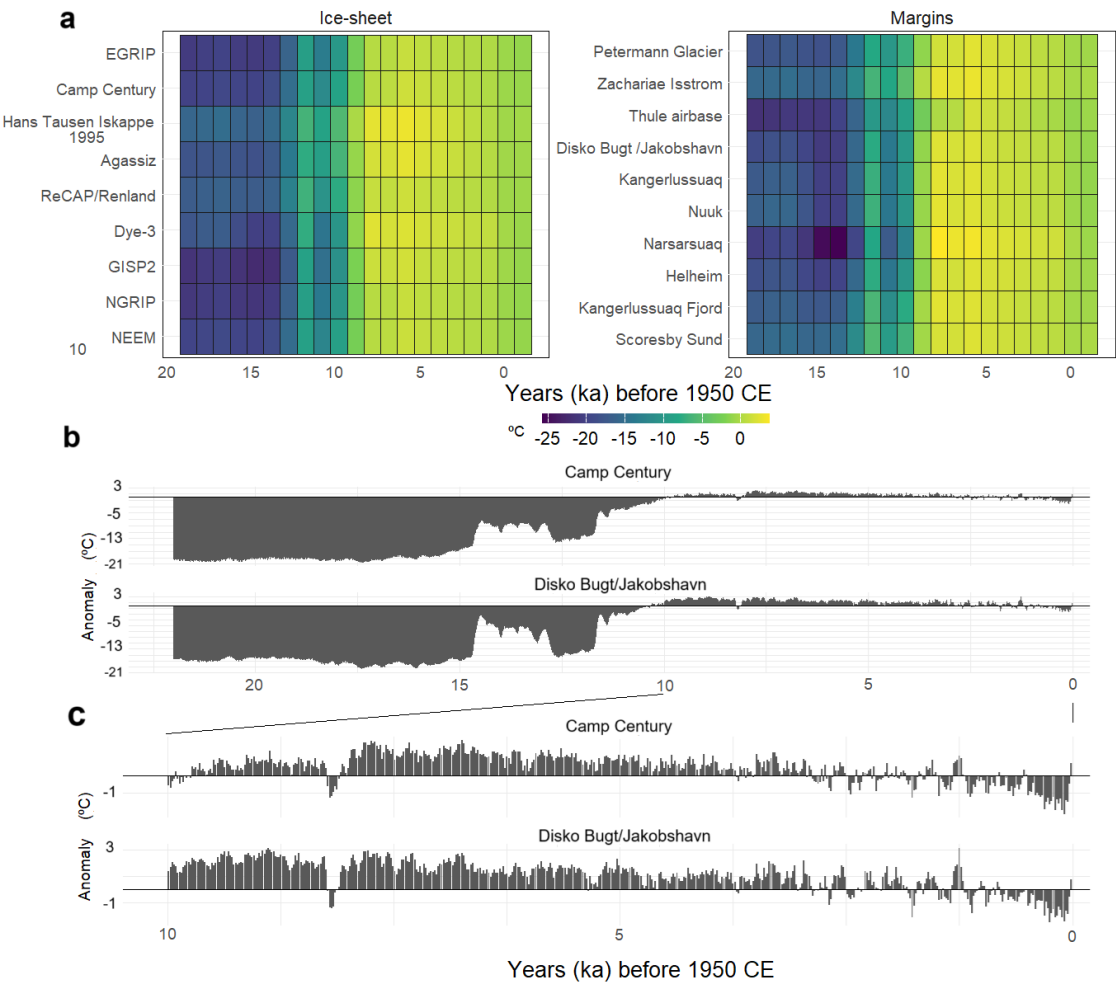


Figure 6. Air temperature anomalies from the LGM period to the present reconstructed from ice-core records of the GrIS and Greenland margins (a). Air temperature anomalies from the ice cores near to the glacier reconstructed in Central-Western Greenland (Camp Century and Disko Bugt/Jakobshavn) (b). The black squares highlighted in (a) correspond to the specific locations shown in (b). Air temperature anomalies since 10 ka to 1950 (c). Air temperature anomalies are calculated by the difference between the average annual air temperature from the baseline climate (1960-1990 period) and the annual air temperature for each location. Data were obtained from the reconstruction available from Buizert et al. (2018).

Future CMIP6 SSP2-4.5 and SSP5-8.5 anomalies with respect to the baseline climate are shown in Figure 7. The temporal evolution of temperature follows a similar warming rate for both scenarios until 2040, after which there is an acceleration of warming for SSP5-8.5. The increase in temperature relative to the baseline climate for SSP2-4.5 is 3.1°C by 2050 and 4.2°C by 2100, whereas for SSP5-8.5, is 3.4°C by 2050 and 6.1°C by 2100. Thus, CMIP6 (SSP2-4.5 and SSP5-8.5) anomalies with respect to the baseline climate are similar to HWP for 2050 but higher by a factor of three for SSP5-8.5 by 2100 (Figure 6). Precipitation also shows an increase with respect to the baseline climate, which is more pronounced for SSP5-8.5 towards the end of the 21st century. SSP2-4.5 precipitation anomalies with respect to the baseline climate are +20% by 2050, increasing to +26% by 2100. For SSP5-8.5, precipitation increases by +20% by 2050 and +38% by 2100.

For the 2050-2060 period, summer temperatures are projected to range from 2°C under SSP2-4.5 to 3°C under SSP5-8.5. For the 2090-2100 period, winter temperatures are projected to range from 5°C under SSP2-4.5 to 8°C under SSP5-8.5 (Figure S3). Regarding snowfall and for the 2050-2060 period, SSP2-4.5 and SSP5-8.5 projects anomalies of 12% and 16 %, respectively (Figure S4 and S5). For the 2090-2100 period, anomalies with respect to the baseline climate are 18 % and 22% for SSP2-4.5 and SSP5-8.5, respectively. Other months show decreases in snowfall except for Spring, which shows a 3% increase for both SSP5-8.5 and SSP2-4.5 scenarios for 2050-2060 and 2090-2100 periods.

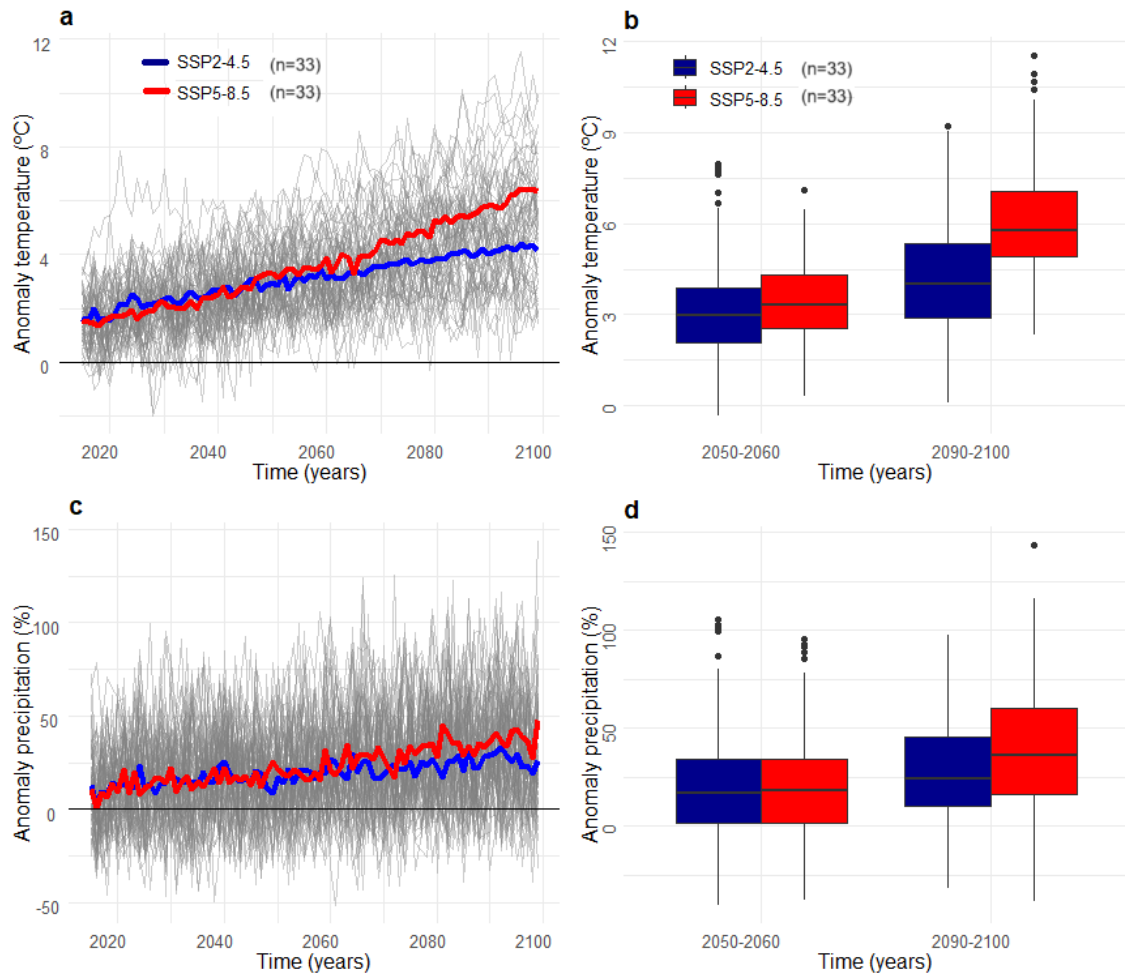


Figure 7. Temporal evolution of CMIP6 SSP2-4.5 and SSP5-8.5 temperature anomalies with respect to the baseline climate period (a). Comparison of CMIP6 SSP2-4.5 and SSP5-8.5 temperature anomalies with respect to the baseline climate period for 2050-2060 and 2090-2100 temporal periods (b). Figure 7 (c) and (d) are the same as Figure 7 (a) and (b), respectively, but for precipitation. The dots of (b) and (d) represent the average of each CMIP6 model for the temporal period and climate variable.

We further assessed whether the temperature conditions reconstructed from ice-core data are consistent with CRE dates from moraine boulders and can accurately replicate the MIE of the Late Holocene. A sensitivity analysis of temperature and precipitation was conducted. For the calibrated melt rate, temperature variations ranged from -1°C to 0°C in 0.25°C increments. For the low-end melt rate, temperature variations ranged from 0.25°C to $+1.25^{\circ}\text{C}$ in 0.25°C increments. Precipitation remained unchanged (0%) or increased by 10%. We determined the temperature and precipitation conditions that allowed the MIE of the Late Holocene glacier extension, enabling its reconstruction (Figure 8).

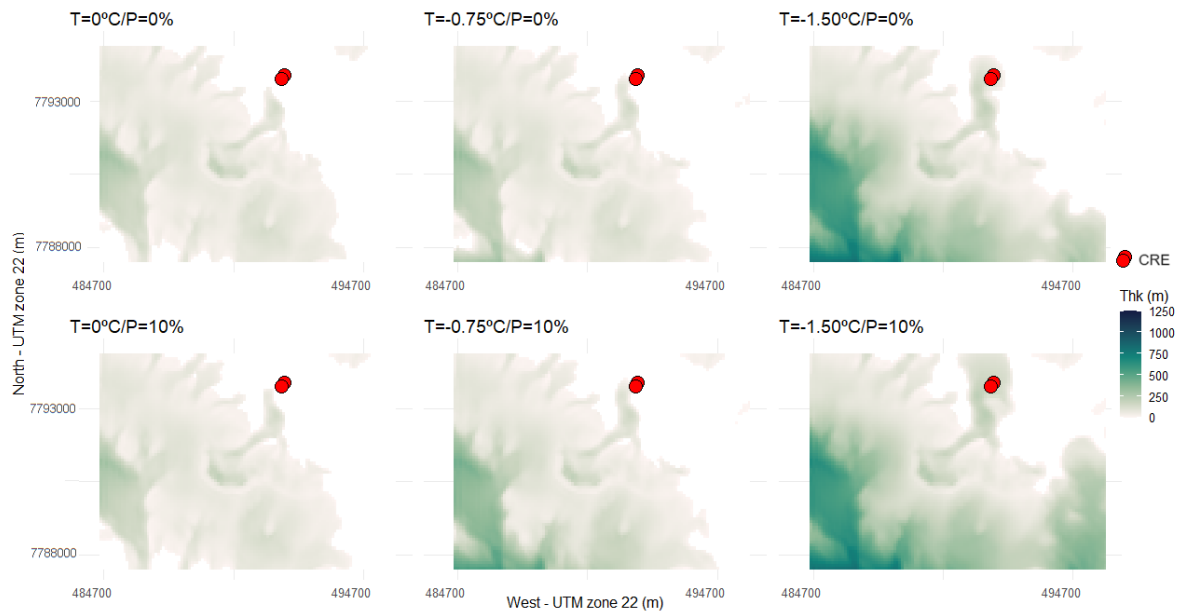
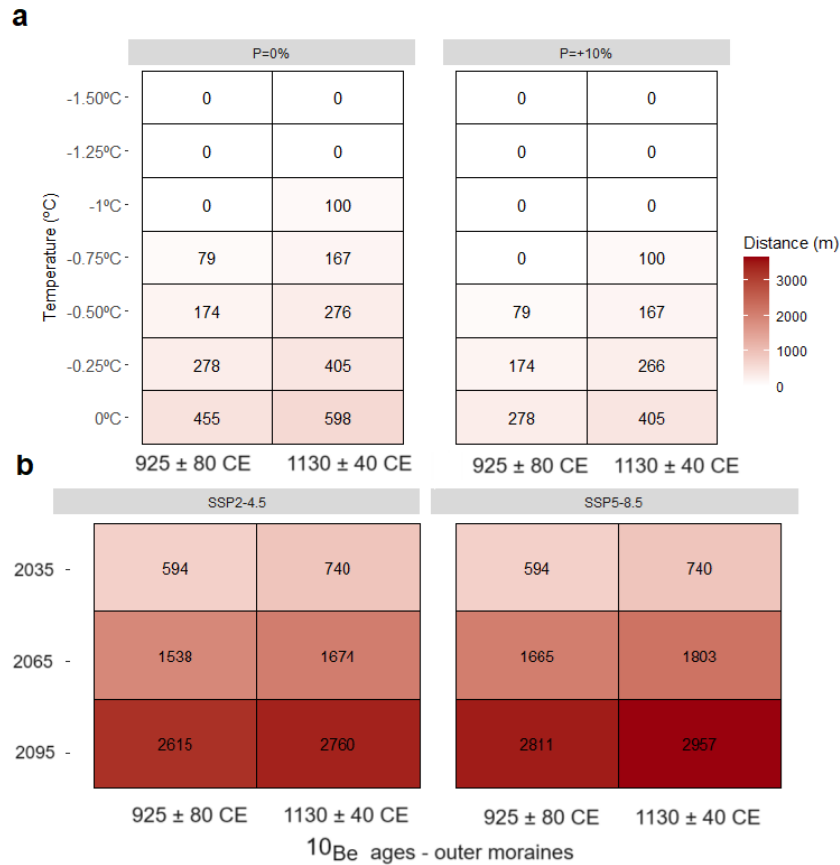


Figure 8. Location of the CRE samples (red dots) and average ice thickness (m) for various temperature (T) and precipitation (P) perturbations. The ice thickness values presented result from an initial spin-up model run, followed by a 1000-year model run to reconstruct the MIE of the Late Holocene. Data are shown for the calibrated IGM configuration and melt rate value. Reconstruction using the IGM default configuration and past reconstruction values with a low-end melt rate are shown in Figures S6 and S7.

The assessment of past temperature and precipitation anomalies relative to the baseline climate is conducted based on the distance between the glacier tongue and available CRE dates. This analysis indicates the temperature and precipitation conditions that facilitated glacier expansion during the MIE of the Late Holocene. Note that there may be a time gap between MIE of the Late Holocene the timing of maximum ice expansion and CRE ages and the since these ages indicate not the period of glacial growth but rather the period when moraine boulders stabilized after the formation of the moraine ridges formed by the glacier advances/stillstands. Assuming a calibrated melt rate, the minimum distance for all samples is reached when the temperature is reduced by 1°C while precipitation remains unchanged. Similarly, a 0.75°C temperature reduction combined with a 10% increase in precipitation relative to the baseline climate also leads to glacier advances reaching the limit marked by the dated moraine boulders (Figures 8 and 9). These findings suggest that temperature anomalies leading to glacier extension up to the MIE of the Late Holocene ranged at least from temperatures of -0.75°C and precipitation of +10% to temperatures of $\leq -1^\circ\text{C}$ and precipitation of 0% relative to the baseline climate (Figure 9). However, a variation in precipitation of 10% is unlikely according to paleoclimate reconstructions for the Late Holocene (Badgeley et al., 2020). This suggests that using a calibrated melt rate factor a temperature between 0.75°C and 1°C from the baseline climate, with no changes in precipitation, is the most plausible climate scenario.



465

466 **Figure 9.** Differences in pixel distance (m) between the nearest modelled glacier
 467 extension and the sample age location (x-axis) across various air temperature (y-axis) and
 468 precipitation options (boxes) (a) using a calibrated melt rate. Differences in pixel distance
 469 (m) between the nearest modelled glacier extension and the sample age location (x-axis)
 470 and projected glacier shrinkage for CMIP6 scenarios (boxes) and different years (y-axis).
 471 Despite the model being calibrated and validated with three independent sources (Figures
 472 2–5), an uncertainty estimation of ice thickness and glaciated area changes was
 473 performed. This estimation was based on variations in the melt rate, the ice-dynamics
 474 IGM configuration, and the temperature lapse rate (Figures S6–S9). The highest
 475 uncertainty (5%) is attributed to the melt rate factor. The glaciated area and ice thickness
 476 have decreased by $15 \pm 5\%$ (Figure 10) compared to the glacier-covered surface during the
 477 MIE of the Late Holocene, where the standard deviation (\pm) accounts for the influence of
 478 the calibrated (-20.1% ice-thickness anomaly) and low-end melt rate factors (15.2%). A
 479 detailed secondary analysis was conducted by comparing the calibrated and default IGM
 480 configurations. The calibrated IGM configuration, along with the default A and c
 481 parameters, results in minor changes (<4%) in ice thickness anomalies while maintaining
 482 the same temperature offsets (Figures S6, S7). Furthermore, a sensitivity analysis of the
 483 temperature lapse rate before bias correction shows small variations in ice-thickness
 484 anomalies relative to the present day. A lower lapse rate (-0.55°C/m), the applied lapse
 485 rate (-0.65°C/m), and a higher lapse rate (-0.75°C/m) result in a 3% difference in ice
 486 thickness anomaly (Figure S8). **5.3 Future glacier changes**

Assuming a calibrated melt rate factor, the future climate for 2060 leads to glacier tongue recession ranging from 1674 m (SSP2-4.5) to 1903 m (SSP5-8.5) relative to the MIE of the Late Holocene (Figures 9 to 11). By 2090, glacier reduction is projected to reach up to 2760 m (SSP2-4.5) or 2957 m (SSP5-8.5). The rate of ice loss from the MIE of the Late Holocene to the present ($15\pm5\%$) will more than double ($40\pm9\%$) after the 2030-2040 period (Figure 10), regardless of the CMIP6 scenario, with the standard deviation (\pm) reflecting the influence of the melt rate factor. By 2070-2080, ice loss will accelerate further, reaching anomalies of $-56\pm6\%$ (SSP5-8.5). By 2100, under SSP5-8.5, ice thickness will decline to a maximum loss leading to the disappear the glaciated area (Figures 11, S10 and S11).

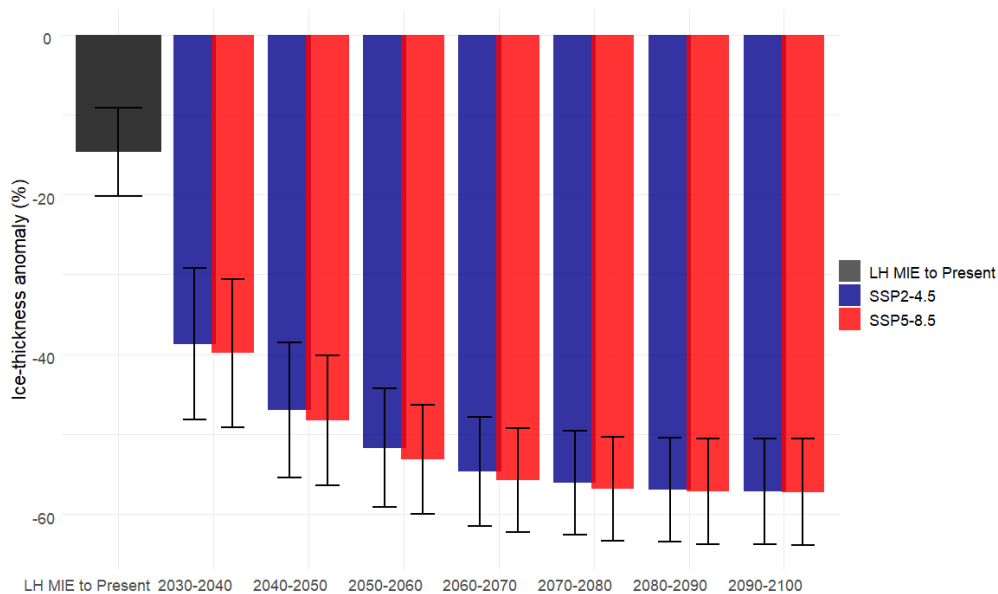


Figure 10. Ice thickness anomalies with respect to present-day glaciated area for the MIE of the Late Holocene (LH) and future CMIP6 SSP2-4.5 and SSP5-8.5 scenarios. The anomaly in ice thickness is calculated by taking the difference between the MIE of the Late Holocene and future ice-loss changes and the present-day accumulated yearly ice thickness. This difference is then divided by the present-day accumulated yearly ice thickness and multiplied by 100. The column bars represent the mean ice thickness anomalies, whereas the error bars represent the standard deviation of the anomalies, which reflect the variability associated with the different melt rate factors.

The

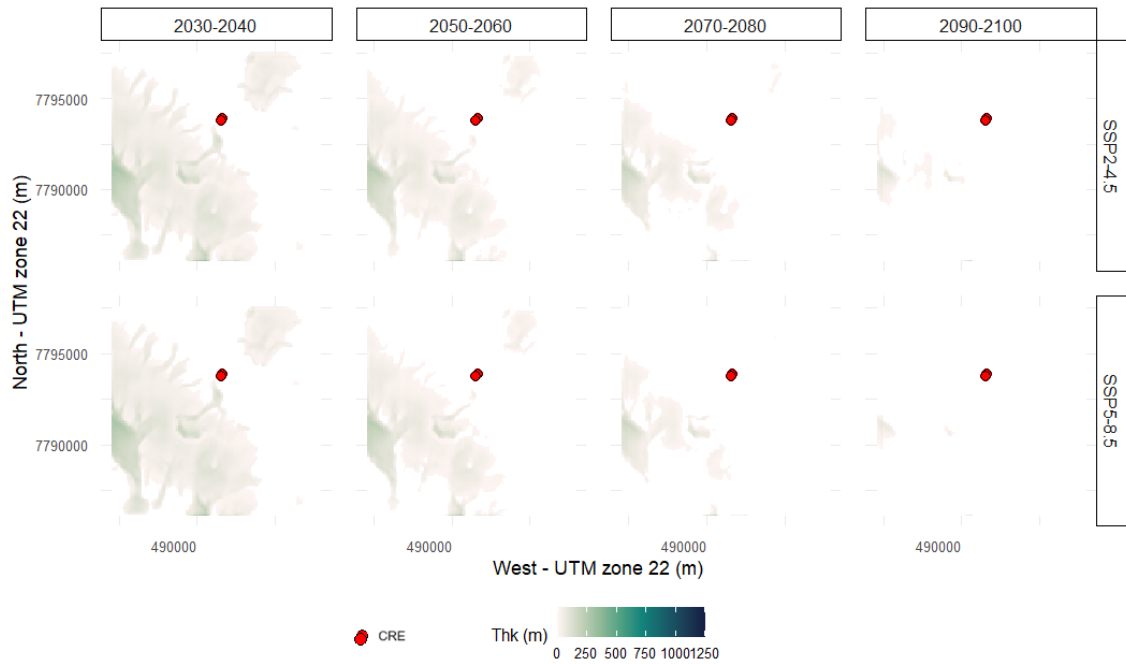


Figure 11. Location of the CRE samples (red dots) and average ice thickness (m) for future CMIP6 SSP2-4.5 and SSP5-8.5 scenarios and different temporal periods. The ice thickness values shown are the result of performing a spin-up model run reaching steady state conditions, and subsequently performing a model run with CMIP6 projections from present-day to 2100. Data are shown for the calibrated IGM configuration and melt rate value. Future simulations using the IGM default configuration and a high-end melt rate are shown in Figures S10 and S11.

6. Discussion

6.1 Glacier modelling as a tool to understand paleoclimate conditions

The range of temperature decrease (0.75°C to 1°C) that obtained the best results in terms of reproducing glacier's MIE of Late Holocene area is consistent with past temperature anomalies in the Western and Southern Greenland found in previous works. Particularly, this range of temperature anomalies fall between estimates of $\sim 1.5^{\circ}\text{C}$ cooler temperature at 1850 CE with respect to 1990s (Dahl-Jensen et al., 1998). In Southern-Western Greenland, temperature estimates derived from geospatial reconstruction of ELAs that attributed historical MIE to the LIA, suggest temperatures ranging from around -0.4 to -0.9°C (Larocca et al., 2020). Employing a similar methodology, other studies have found temperature anomalies during the LIA to be of $-1.1 \pm 0.6^{\circ}\text{C}$, with no observed changes in precipitation (Brooks et al., 2022).

However, the MIE of the Late Holocene in Central-Western Greenland defined by the most recent moraine complexes suggest an earlier maximum glacier extent than in other areas in the Northern Hemisphere when the LIA glacier expansion was much more extensive (Young et al., 2015). In this sense, the temperature indicated by at Northern-Hemispheric scale reanalysis for the MWP is not consistent with MIE obtained from

glacier moraines dated with CRE in Western Greenland (Jomelli et al., 2016; Biette et al., 2019). Indeed, Biette et al. (2019) modelled the outlet glacier of the Lyngmarksbræen ice cap (Disko Island) and tested its sensitivity to temperature and precipitation using a PDD approach guided by temperature anomalies from a lake sediment located 250 km south of Disko Island (D'Andrea et al., 2011). They demonstrated that the MIE of the Late Holocene during the late MWP (1200 ± 130 CE) occurred when temperatures ranged from -1.3°C to -1.6°C , and precipitation changed by $\pm 10\%$ (Biette et al., 2019). Considering that the baseline climate period of our work is 1960 to 1990, and their anomalies are considered to the end-20th century, our results are similar to these reported temperature and precipitation values. These results are in line with a decrease in summer temperature from -0.5° to -3°C at around 250 km of Disko Island during the MWP obtained from lacustrine (alkenone-based lake sediment) reconstructions, and a second cold phase during the LIA (D'andrea et al., 2011). These cold conditions have been linked to multi-decadal cold spells intense enough to cause a major advance of Baffin Bay during the MWP (Young et al., 2015; Jomelli et al., 2016). These glacier advances were also observed in other Northern Hemisphere glaciers and may be also enhanced by volcanic eruptions (Solomina et al., 2016). The reconstructed glacier advances were probably linked with a recurrent positive NAO at West Greenland and Baffin Bay during MWP that lead to cool conditions (Young et al., 2015). However, other studies suggested that the NAO was not predominantly positive during this period (Lasher and Axford, 2019). There are also studies suggesting cold sea-surface temperatures observed during the MWP (Sha et al., 2017), while others suggest warmer conditions during the MWP compared to the LIA (Perner et al., 2012).

The MIE of the glaciers in the study area was reached during the MWP (1130 ± 40 and 925 ± 80 CE) (Young et al., 2015), has been suggested to be linked to increased snowfall rates that counterbalanced the glacier ablation mass losses during the MWP, which were slightly higher than those during the LIA (Osman et al., 2021). However, an increase of precipitation of $+ 10 \%$ with respect to the baseline climate period is not able to counterbalance glacier recession under a change of $<-0.5^{\circ}\text{C}$ with respect to the baseline climate (Figure 9). The sensitivity analysis performed here reveals that the glaciated area was not in isothermal conditions within 1960-1990 period and a small decadal variation of temperature with respect to the baseline analysis to temperature and precipitation performed in this work is consistent with previous works that suggest that around 90% of variation and that glacier maximum extension dynamics are linked with summer temperature (Miller et al., 2012; Young et al., 2015).

6.2 Central-Western Greenland ice-loss and comparison with other Greenland areas

The reconstructed MIE of the Late Holocene represents the phase with most recent widespread glacier advances from the Nuussuaq Peninsula, and it occurred prior to the LIA (Schweinsberg et al., 2017; 2019). The maximum glacier advance reconstructed in this work for Central-Western Greenland is not consistent across Greenland. Northern GrIS exhibits stability during the Late Holocene with advances at 2.8 ka and 1650 CE

(Reusche et al., 2018). In particular, North-Western glaciers length was similar from 5.8 ka until onset of LIA (Søndergaard et al., 2020). In the Bregne Ice Cap (East Greenland) glacier length dating reveals a peak during the LIA (~ 0.74 ka; Levy et al., 2014). However, in Renland Ice Cap (Eastern Greenland) glaciers exceeded present limits at 3.3 ka and around 1 ka, which is similar to LIA glacier advance (Medford et al., 2021). In Central-East Greenland, cold climate conditions occurred during LIA at Stauning Alper with peaks of 0.78 ± 0.31 ka (Kelly et al., 2008), and at Istorvet ice cap, that reached its maximum Holocene extent at 0.8 ± 0.3 ka (Lowell et al., 2013). This expansion observed in Eastern Greenland corresponds with peak glacier extensions seen in Iceland, attributed to LIA (Flowers et al., 2008). Different asymmetries between Greenland sectors are seen historically as revealed by long-term GICs recession larger in West Greenland than in East, which has been attributed to the positive oscillation of NAO since the LIA that led to warmer conditions in West Greenland due to the West-East NAO dipole (Bjørk et al., 2018).

In Central-Western Greenland, most of the studies focusing on Late Holocene glacial history come from near Disko Island (Ingolfsson et al., 1990; Humlum, 1998; Yde and Knudsen, 2007; Citterio et al., 2009; Jomelli et al., 2016). Here, in its Eastern fringe, the ELA from the LIA is estimated at ca. 550 ± 500 m, contrasting with values of 200-300 m attributed elsewhere in the island (Ingolfsson et al., 1990). In the Western section, however, the ELA during the LIA was estimated to be at 450 ± 420 m (Humlum, 1998). As in Nuussuaq Peninsula, the Holocene maximum extension in Disko Island is evidenced by moraine systems exhibiting a fresh, partly unvegetated appearance, with prevalence of *Rhizocarpon geographicum* in these moraines (Humlum, 1987). This absence of Holocene moraine systems beyond the LIA moraines indicates that the advance of LIA represents the maximum extension of this glacier since the Late Holocene (Humlum, 1999). This moraine evidence has been used to estimate the ELA (Brooks et al., 2022; Carrivick et al., 2023). Particularly, using geospatial methods Carrivick et al. (2023) attributed this trimline to the maximum extent of LIA and concluded that Greenland GICs lost 499 Gt since end-LIA, corresponding to 1.38 mm sea level equivalent. Similarly, in Southern-Western Greenland, 42 GICs lost 48% of their area since the LIA with respect to 2019 (Brooks et al., 2022). These values are higher than the 15 ± 5 % ice-thickness reduction from the MIE of the Late Holocene with respect to present-day glaciated area reported in this work. The differences could be attributed to the local relief configuration as well as to the north aspect of the reconstructed glacier area and methodological variances. Additionally, while we are employing a glacier modelling approach constrained by geological records of a specific age, previous studies have estimated distances based on ELAs and geospatial methods that account for spatial distances between present-day glaciers tongue and maximum historical moraines that could be formed prior to the LIA. According to remote sensing data, in Disko Island GICs inventory and monitoring from 1953 to 2005 indicates that the average recession during this timeframe amounted to 11% of the glacier lengths recorded in 1953 (number of glaciers, $n = 172$), and 38% of the distance between LIA moraines and glacier termini in

1953 ($n = 87$) (Yde and Knudsen, 2007). These values are lower than those observed at Pjetursson Glacier (Disko Island), which has retreated since the LIA with a decrease in total glacier area of around 40% by the end of the 20th century according to geospatial methods (Bøcker, 1996). Using remote sensing data, LIA to 2001 glacier shrinkage in Central-Western Greenland was estimated in a reduction of $\sim 20\%$ of the area (Citterio et al., 2009).

Currently, the modeled glaciated area and volume are out of balance with respect to the temperature since 1990 to present (figure not shown), necessitating the simulation the glaciated area using temperature and precipitation data from the 1960-1990 period (Figure 2). This indicates a committed ice loss regardless of future climate scenarios. Future projections show a remarkable increase in temperature, reaching HWP anomalies by 2050 and tripling HWP anomalies by 2100 under SSP5-8.5. Our results indicate that glacier mass loss by >2070 will double the ice loss from the MIE of the Late Holocene to the present. Precipitation is projected to increase by 20% (2050; SSP2-4.5 and SSP5-8.5) up to 38% (2100; SSP5-8.5) compared to the baseline climate but cannot counterbalance glacier losses, and the modeled glaciated area is expected to disappear by 2090-2100 (Figure 11). The data presented in this work suggests that future glacier ice loss will occur at unprecedented rates compared to the period from the MIE of the Late Holocene to the present.

According to CMIP6 projections for near-ice-free zones of Disko Island, this temperature increase is explained by increases in long-wave radiation and slight variations or decreases in short-wave radiation (Bonsoms et al., 2024). Future winter temperatures are expected to remain below isothermal conditions, leading to more snowfall during winter (i.e., +22% for SSP5-8.5 for the 2090-2100 period, relative to the baseline climate). The increase of snowfall, however, cannot counterbalance glacier shrinkage, and a 10% increase in precipitation has minimal impact on glacier area and thickness variability (Figure 8). Snowpack projections for a near-ice-free region of Disko Island align with these findings, indicating decreases in snow depth and snowfall fraction, along with increases in snow ablation (Bonsoms et al., 2024a). For the GrIS, previous studies projected a larger SMB decrease in ice sheet margins due to higher melting and lower accumulation compared to the GrIS interior; pointing out that increases in snowfall are insufficient to counterbalance the increased runoff (Fettweis et al., 2013). Yet, CMIP6 models are unable to capture the increase in anticyclonic events in Greenland since 1990s (Delhasse et al., 2021), which have driven increased melting and extreme melting events in the GrIS (Bonsoms et al., 2024).

Greenland GICs numerical modelling reconstructions are scarce in comparison with GrIS numerical modelling works; including paleoclimate modelling (Huybrechts, 2002), model parameters sensitivity studies (Cuzzone et al., 2019) or GrIS Holocene evolution constrained with geological records (i.e., Simpson et al., 2009; Lecavalier et al., 2014, Briner et al., 2020). GICs make a modest (11 %) contribution to total Greenland ice loss but exhibit a fast response to warming (Khan et al., 2019). While we modeled the response

of a glaciated area in Eastern Nuussuaq, future studies should compare these ice loss rates with GrIS trends, which exhibit a slower response to warming (Ingolfsson et al., 1990). The anticipated glacier retreat has important environmental implications, including increased freshwater release into the North Atlantic and alterations in atmospheric and circulation patterns (Yu and Zhong, 2018), which may impact the Atlantic Meridional Overturning Circulation (Thornalley et al., 2018). Thus, Greenland glacial retreat, snow melting, and permafrost thaw will amplify greenhouse gases release and potentially trigger major consequences at global scale (Miner et al., 2022). Negative mass balances will change geomorphological and permafrost patterns (Christiansen et al., 2010) and ecosystem dynamics in ice-free zones, by modifying maritime (Saros et al., 2019), and terrestrial phenological and fauna distribution (John Anderson et al., 2017).

6.3 Atmospheric forcing and numerical modelling considerations

This work is based on GSWP3 W5E5v2.0 climate dataset, which is based on ERA5 reanalysis data bias-adjusted over land (Lange et al., 2021). ERA5 incorporates observations via a data-assimilation system combining observations, modelling, and satellite data, and was previously validated in Greenland (Delhasse et al., 2020). ERA5 has been used to force state-of-the-art regional climate models, showing good agreement with observations (Box et al., 2022). Our results are consistent with previous works that provided a glacier reconstruction based on outputs of MAR forced with ERA5 and a PDD model in Disko Island (Central-Western Greenland) (Biette et al., 2019). Results are indeed similar to geo-spatial reconstructions in other Greenland sectors (i.e., Brooks et al., 2022). The main conclusions of this work are consistent with paleo GrIS reconstructions and projections in Central-Western GrIS (Briner et al. 2020).

A more sophisticated glacier modelling experiment will require data from coupling regional circulation models, which account for changes in large-scale circulation. However, glacier modelling driven by paleoclimate simulations has uncertainties and large variability between models, as previous works in the study area have shown that paleoclimate simulations cannot reconstruct Late Holocene glacier dynamics in the study area (Jomelli et al., 2016; Biette et al., 2019). In this work a sensitivity analysis to precipitation and temperature is conducted to reconstruct glacier MIE based on cosmogenic data, and therefore results are analyzed based on anomalies with respect to a baseline climate (1960-1990), which is sufficiently long to consider climate interannual variability and is marginally affected by climate warming.

IGM has been previously validated for modelling the present and projecting the future evolution of alpine glaciers, providing reliable results (Cook et al., 2023; and references therein). Here we have performed a IGM parameter tuning to accurately simulate present-day glacier conditions. We cross validated results against two independent ice thickness products (Farinotti et al., 2019; Millan et al., 2022) and RGI6.0 observations. Data shows good agreement when compared to Farinotti et al. (2019) but lesser agreement against Millan et al. (2022) (Figure 4). These differences could be attributed to the different glacier methodologies: Farinotti et al. (2019) is based on an ensemble of five glacier

models founded on ice flow physics, whereas Millan et al. (2022) is based on glacier flow mapping. Further research should analyze these differences. As most numerical modelling experiments, past and future ice flow parameters are likely different from present-day parameters due to unknown variables such as variations in basal conditions, bedrock topography, and ice rheology. This issue was minimized by analyzing glacier simulations using both the IGM default configuration and a calibrated IGM option, validated against available mass balance data, observations, and ice-thickness products. This approach allowed for isolating and better analyzing the effects of temperature and precipitation on past and future glacier trends.

As with most paleo glacier models, IGM relies on a PDD approach, which is an approximation that does not account for the Surface Energy Balance (SEB) driving melting. However, the SEB components required for glacier modelling are uncertain for the spatial and temporal scales analyzed in this study. PDD is based on a temperature index model. Impurities on the ice (such as algae, dust, etc.) are not directly considered but indirectly inferred by the melt rate factor. The IGM configuration for the calibration and correction process of precipitation and temperature is based on OGGM v1.6.1 (Maussion et al., 2015; Schuster et al., 2023). This calibration corrects precipitation and temperature to match geodetic mass balance at the glacier level (Hugonnet et al., 2021). This product was selected due to the lack of long-term past and present in-situ mass balance measurements in the study area. Errors of Hugonnet et al. (2021) product are therefore influencing the glacier modelling results when using the calibrated melt rate factor. The OGGM v1.6.1 calibration of bias correction has been recently compared and cross-validated for glacier modelling of past and future glacier projections, demonstrating reliable results (i.e., Aguayo et al., 2023; Zekollari et al., 2024, and references therein). Additionally, we addressed uncertainties in temperature lapse rates and PDD calibration by incorporating both low-end and high-end melt rate factors, providing a confidence interval for past and future simulations.

7. Conclusions

This study provides a long-term perspective on the dynamics of Eastern Nuussuaq, Central-Western Greenland's GICs in response to climate change. By integrating geological records, ice thickness estimates, and climate model projections, we contextualize present and future glacier loss within the Late Holocene.

The IGM was calibrated and validated using various parameterizations to accurately simulate glacier ice thickness and area. After a long-term spin-up simulation, the model stabilized, closely matching available ice thickness data and satellite observations from RGI6.0. The optimal configuration reproduced ice-thickness estimates with an error of less than 10% of the total accumulated ice thickness for the modelled area. Subsequently, the model was forced with an different temperature and precipitation scenarios, validated with CRE records, enabling the quantification of glacier retreat since the MIE of the Late Holocene. For future projections, IGM was driven by CMIP6 climate scenarios (SSP2-

4.5 and SSP5-8.5), providing a comparative framework for past and future glacier recession in a changing climate. The main conclusions of this study are as follows:

- The MIE of the Late Holocene was reached when temperatures were 0.75°C to 1°C lower than the baseline climate period (1960-1990) under a calibrated melt rate factor.
- Currently, glaciated area ice thickness has retreated by 15% (low-end melt rate) to 20% (calibrated melt rate) compared to the MIE of the Late Holocene.
- Glacier mass loss is projected to occur at an unprecedented rate within the Late Holocene. Future simulations for 2070-2080 indicate a retreat more than double ($-56\pm6\%$) compared to the ice loss from the MIE of the Late Holocene to the present.
- The glaciated area is expected to disappear towards 2090-2100.

Results confirm the ongoing imbalance of Eastern Nuussuaq, Central-Western Greenland GICs and highlight the unprecedented nature of current glacier shrinkage within the Late Holocene. Projections suggest that climate change will accelerate ice loss beyond historical trends, transforming Arctic landscapes, increasing deglaciated areas, and promoting the formation of new lakes. These findings enhance our understanding of Arctic peripheral glacier responses to anthropogenic climate change, with broad implications for hydrological and ecological systems.

Code and data availability

IGM is an open-access model provided at <https://github.com/jouvetg/igm> (Jouvet, 2023a). Data of this work are available upon request to the first author (josepbonsoms5@ub.edu).

Author contributions

JB wrote the manuscript. JB modeled and analyzed the results under the guidance of GJ. JB, MO, JILM, and GJ conceptualized and designed the study. JB, MO, and JILM edited the manuscript and contributed to the discussion of the results. GJ provided feedback on the modeling aspects. MO supervised the project and secured funding. **Competing interests**

The authors have not competing interests.

Acknowledgements

This manuscript falls within the research topics examined by the research group Antarctic, Arctic and Alpine Environments (ANTALP; 2017-SGR-1102) funded by the Government of Catalonia and MARGISNOW (PID2021-124220OB-100), from the Spanish Ministry of Science, Innovation and Universities. Josep Bonsoms is supported by a pre-doctoral FPI grant (PRE2021097046) funded by the Spanish Ministry of Science, Innovation and

Universities. We thank the editor Dr. Florence Colleoni, reviewer Dr. Adriano Ribolini and an anonymous reviewer for their comments that helped to improve the manuscript.

8. References

Aguayo, R., Maussion, F., Schuster, L., Schaefer, M., Caro, A., Schmitt, P., Mackay, J., Ultee, L., Leon-Muñoz, J., and Aguayo, M.: Assessing the glacier projection uncertainties in the Patagonian Andes (40–56° S) from a catchment perspective, <https://doi.org/10.5194/egusphere-2023-2325>, 2024.

Badgeley, J. A., Steig, E. J., Hakim, G. J., and Fudge, T. J.: Greenland temperature and precipitation over the last 20000 years using data assimilation, *Climate of the Past*, 16, 1325–1346, <https://doi.org/10.5194/cp-16-1325-2020>, 2020.

Biette, M., Jomelli, V., Favier, V., Chenet, M., Agosta, C., Fettweis, X., Minh, D.H.T., Ose, K., 2018. Estimation des températures au début du dernier millénaire dans l'ouest du Groenland : résultats préliminaires issus de l'application d'un modèle glaciologique de type degré jour sur le glacier du Lyngmarksbræen. *Géomorphologie Relief Process. Environ.* 24. <https://doi.org/10.4000/geomorphologie.11977>

Bjørk, A. A., Aagaard, S., Lütt, A., Khan, S. A., Box, J. E., Kjeldsen, K. K., Larsen, N. K., Korsgaard, N. J., Cappelen, J., Colgan, W. T., Machguth, H., Andresen, C. S., Peings, Y., and Kjær, K. H.: Changes in Greenland's peripheral glaciers linked to the North Atlantic Oscillation, *Nat Clim Chang*, 8, 48–52, <https://doi.org/10.1038/s41558-017-0029-1>, 2018.

Bøcker, C. A.: Using GIS for glacier volume calculations and topographic influence of the radiation balance. An example from Disko, West Greenland, *Geografisk Tidsskrift*, 100, 11–20, <https://doi.org/10.1080/00167223.1996.10649372>, 1996.

Bolch, T., Sandberg Sørensen, L., Simonsen, S. B., Mölg, N., Machguth, H., Rastner, P., and Paul, F.: Mass loss of Greenland's glaciers and ice caps 2003–2008 revealed from ICESat laser altimetry data, *Geophys Res Lett*, 40, 875–881, <https://doi.org/10.1002/grl.50270>, 2013.

Bonsoms, J., Oliva, M., Alonso-González, E., Revuelto, J., and López-Moreno, J. I.: Impact of climate change on snowpack dynamics in coastal Central-Western Greenland, *Science of the Total Environment*, 913, <https://doi.org/10.1016/j.scitotenv.2023.169616>, 2024a.

Bonsoms, J., Oliva, M., López-Moreno, J. I. and Fettweis, X. Rising extreme meltwater trends in Greenland ice sheet (1950 – 2022): surface energy balance and large-scale circulation changes. *J. Climate*, <https://doi.org/10.1175/JCLI-D-23-0396.1>, in press, 2024b.

Briner, J. P., Cuzzzone, J. K., Badgeley, J. A., Young, N. E., Steig, E. J., Morlighem, M., Schlegel, N. J., Hakim, G. J., Schaefer, J. M., Johnson, J. V., Lesnek, A. J., Thomas, E. K., Allan, E., Bennike, O., Cluett, A. A., Csatho, B., de Vernal, A., Downs, J., Larour, E.,

816 and Nowicki, S.: Rate of mass loss from the Greenland Ice Sheet will exceed Holocene
817 values this century, *Nature*, 586, 70–74, <https://doi.org/10.1038/s41586-020-2742-6>,
818 2020.

819 Brooks, J. P., Larocca, L. J., and Axford: Little Ice Age climate in southernmost Greenland
820 inferred from 1 quantitative geospatial analyses of alpine glacier reconstructions, 2022.

821 Buizert, C., Keisling, B. A., Box, J. E., He, F., Carlson, A. E., Sinclair, G., and DeConto,
822 R. M.: Greenland-Wide Seasonal Temperatures During the Last Deglaciation, *Geophys*
823 *Res Lett*, 45, 1905–1914, <https://doi.org/10.1002/2017GL075601>, 2018.

824 Cappelen, J.: Weather and climate data from Greenland 1958-2011-Observation data with
825 description, n.d.

826 Carrivick, J. L., Boston, C. M., Sutherland, J. L., Pearce, D., Armstrong, H., Bjørk, A.,
827 Kjeldsen, K. K., Abermann, J., Oien, R. P., Grimes, M., James, W. H. M., and Smith, M.
828 W.: Mass Loss of Glaciers and Ice Caps Across Greenland Since the Little Ice Age,
829 *Geophys Res Lett*, 50, <https://doi.org/10.1029/2023GL103950>, 2023.

830 Christiansen, H. H., Etzelmüller, B., Isaksen, K., Juliussen, H., Farbrot, H., Humlum, O.,
831 Johansson, M., Ingeman-Nielsen, T., Kristensen, L., Hjort, J., Holmlund, P., Sannel, A.
832 B. K., Sigsgaard, C., Åkerman, H. J., Foged, N., Blikra, L. H., Pernosky, M. A., and
833 Ødegård, R. S.: The thermal state of permafrost in the nordic area during the international
834 polar year 2007-2009, *Permafr Periglac Process*, 21, 156–181,
835 <https://doi.org/10.1002/ppp.687>, 2010.

836 Citterio, M., Paul, F., Ahlstrøm, A. P., Jepsen, H. F., and Weidick, A.: Remote sensing of
837 glacier change in West Greenland: Accounting for the occurrence of surge-type glaciers,
838 *Ann Glaciol*, 50, 70–80, <https://doi.org/10.3189/172756410790595813>, 2009.

839 Cronauer, S. L., Briner, J. P., Kelley, S. E., Zimmerman, S. R. H., and Morlighem, M.:
840 ¹⁰Be dating reveals early-middle Holocene age of the Drygalski Moraines in central West
841 Greenland, *Quat Sci Rev*, 147, 59–68, <https://doi.org/10.1016/j.quascirev.2015.08.034>,
842 2016.

843 Cucchi, M., P. Weedon, G., Amici, A., Bellouin, N., Lange, S., Müller Schmied, H.,
844 Hersbach, H., and Buontempo, C.: WFDE5: Bias-adjusted ERA5 reanalysis data for
845 impact studies, *Earth Syst Sci Data*, 12, 2097–2120, [https://doi.org/10.5194/essd-12-](https://doi.org/10.5194/essd-12-2097-2020)
846 2097-2020, 2020.

847 Cuzzone, J. K., Schlegel, N. J., Morlighem, M., Larour, E., Briner, J. P., Seroussi, H., and
848 Caron, L.: The impact of model resolution on the simulated Holocene retreat of the
849 southwestern Greenland ice sheet using the Ice Sheet System Model (ISSM), *Cryosphere*,
850 13, 879–893, <https://doi.org/10.5194/tc-13-879-2019>, 2019.

851 Cook, S. J., Jouvet, G., Millan, R., Rabatel, A., Zekollari, H., and Dussailant, I.:
852 Committed Ice Loss in the European Alps Until 2050 Using a Deep-Learning-Aided 3D

853 Ice-Flow Model With Data Assimilation, *Geophys Res Lett*, 50,
854 <https://doi.org/10.1029/2023GL105029>, 2023.

855 D'andrea, W. J., Huang, Y., Fritz, S. C., and Anderson, N. J.: Abrupt Holocene climate
856 change as an important factor for human migration in West Greenland,
857 <https://doi.org/10.1073/pnas.1101708108/-/DCSupplemental>, 2011.

858 Erokhina, O., Rogozhina, I., Prange, M., Bakker, P., Bernales, J., Paul, A., and Schulz,
859 M.: Dependence of slope lapse rate over the Greenland ice sheet on background climate,
860 *J. Glaciol.*, 63, 568–572, <https://doi.org/10.1017/jog.2017.10>, 2017.

861 Farinotti, D., Huss, M., Fürst, J.J. et al. A consensus estimate for the ice thickness
862 distribution of all glaciers on Earth. *Nat. Geosci.* 12, 168–173,
863 <https://doi.org/10.1038/s41561-019-0300-3>, 2019.

864 Flowers, G. E., Björnsson, H., Geirsdóttir, Á., Miller, G. H., Black, J. L., and Clarke, G.
865 K. C.: Holocene climate conditions and glacier variation in central Iceland from physical
866 modelling and empirical evidence, *Quat Sci Rev*, 27, 797–813,
867 <https://doi.org/10.1016/j.quascirev.2007.12.004>, 2008.

868 Glen, J. W. The Creep of Polycrystalline Ice, *Proceedings of the Royal Society of London.*
869 *Series A, Mathematical and Physical Sciences* (1934-1990), 228(1175), 519538,
870 doi:10.1098/rspa.1955.0066, 1955.

871 Hanna, E., Huybrechts, P., Janssens, I., Cappelen, J., Steffen, K., and Stephens, A.: Runoff
872 and mass balance of the Greenland ice sheet: 1958–2003, *J. Geophys. Res.*, 110,
873 D13108, <https://doi.org/10.1029/2004JD005641>, 2005.

874 Hanna, E., Mernild, S. H., Cappelen, J., and Steffen, K.: Recent warming in Greenland in
875 a long-term instrumental (1881-2012) climatic context: I. Evaluation of surface air
876 temperature records, *Environmental Research Letters*, 7, [https://doi.org/10.1088/1748-](https://doi.org/10.1088/1748-9326/7/4/045404)
877 [9326/7/4/045404](https://doi.org/10.1088/1748-9326/7/4/045404), 2012.

878 Hansen, B. U., Elberling, B., Humlum, O., and Nielsen, N.: Meteorological trends (1991-
879 2004) at Arctic Station, Central West Greenland (69°15'N) in a 130 years perspective,
880 *Geografisk Tidsskrift*, 106, 45–55, <https://doi.org/10.1080/00167223.2006.10649544>,
881 2006.

882 Helama, S., Jones, P. D., and Briffa, K. R. Dark Ages Cold Period: A literature review and
883 directions for future research. *The Holocene*, 27(10), 1600-1606.
884 <https://doi.org/10.1177/0959683617693898>, 2017.

885 Hock, R.: Temperature index melt modelling in mountain areas, *J Hydrol (Amst)*, 282,
886 104–115, [https://doi.org/10.1016/S0022-1694\(03\)00257-9](https://doi.org/10.1016/S0022-1694(03)00257-9), 2003.

887 Hugonnet, R., McNabb, R., Berthier, E., Menounos, B., Nuth, C., Girod, L., Farinotti, D.,
888 Huss, M., Dussallant, I., Brun, F., and Käab, A.: Accelerated global glacier mass loss in

889 the early twenty-first century, *Nature*, 592, 726–731, [https://doi.org/10.1038/s41586-021-](https://doi.org/10.1038/s41586-021-03436-z)
890 03436-z, 2021.

891 Humlum, O.: The climatic significance of rock glaciers, *Permafrost Periglacial Process*, 9, 375–
892 395, [https://doi.org/10.1002/\(SICI\)1099-1530\(199810/12\)9:4<375::AID-](https://doi.org/10.1002/(SICI)1099-1530(199810/12)9:4<375::AID-PPP301>3.0.CO;2-0)
893 PPP301>3.0.CO;2-0, 1998.

894 Humlum, O.: Late-Holocene climate in central West Greenland: meteorological data and
895 rock-glacier isotope evidence, *The Holocene*, 581–594 pp., 1999.

896 Huss, M., Bauder, A., Funk, M., and Hock, R.: Determination of the seasonal mass
897 balance of four Alpine glaciers since 1865, *J Geophys Res Earth Surf*, 113,
898 <https://doi.org/10.1029/2007JF000803>, 2008.

899 Ingolfsson, O., Frich, P., Funder, S., and Humlum O, O. B.: 12 01: Paleoclimatic
900 implications of an early Holocene glacier advance on Disko Island, West Greenland.
901 *Boreav*, 297–311 pp., 1990.

902 IPCC: High Mountain Areas, in: *The Ocean and Cryosphere in a Changing Climate*,
903 Cambridge University Press, 131–202, <https://doi.org/10.1017/9781009157964.004>,
904 2022.

905 Jiang, S., Ye, A., and Xiao, C.: The temperature increase in Greenland has accelerated in
906 the past five years, *Glob Planet Change*, 194,
907 <https://doi.org/10.1016/j.gloplacha.2020.103297>, 2020.

908 John Anderson, N., Saros, J. E., Bullard, J. E., Cahoon, S. M. P., McGowan, S., Bagshaw,
909 E. A., Barry, C. D., Bindler, R., Burpee, B. T., Carrivick, J. L., Fowler, R. A., Fox, A. D.,
910 Fritz, S. C., Giles, M. E., Hamerlik, L., Ingeman-Nielsen, T., Law, A. C., Mernild, S. H.,
911 Northington, R. M., Osburn, C. L., Pla-Rabès, S., Post, E., Telling, J., Stroud, D. A.,
912 Whiteford, E. J., Yallop, M. L., and Yde, A. J. C.: The arctic in the twenty-first century:
913 Changing biogeochemical linkages across a paraglacial landscape of Greenland,
914 <https://doi.org/10.1093/biosci/biw158>, 1 February 2017.

915 Jomelli, V., Lane, T., Favier, V., Masson-Delmotte, V., Swingedouw, D., Rinterknecht, V.,
916 Schimmelpfennig, I., Brunstein, D., Verfaillie, D., Adamson, K., Leanni, L., Mokadem,
917 F., Aumaître, G., Bourlès, D. L., and Keddadouche, K.: Paradoxical cold conditions
918 during the medieval climate anomaly in the Western Arctic, *Sci Rep*, 6,
919 <https://doi.org/10.1038/srep32984>, 2016.

920 Jouvét, G.: Inversion of a Stokes glacier flow model emulated by deep learning, *Journal*
921 *of Glaciology*, 69, 13–26, <https://doi.org/10.1017/jog.2022.41>, 2023a.

922 Jouvét, G., Cordonnier, G., Kim, B., Lüthi, M., Vieli, A., and Aschwanden, A.: Deep
923 learning speeds up ice flow modelling by several orders of magnitude, *Journal of*
924 *Glaciology*, 68, 651–664, <https://doi.org/10.1017/jog.2021.120>, 2022.

925 Jouvett, G., Cohen, D., Russo, E., Buzan, J., Raible, C. C., Haeberli, W., Kamleitner, S.,
 926 Ivy-Ochs, S., Imhof, M. A., Becker, J. K., Landgraf, A., and Fischer, U. H.: Coupled
 927 climate-glacier modelling of the last glaciation in the Alps, *Journal of Glaciology*,
 928 <https://doi.org/10.1017/jog.2023.74>, 2023b.

929 Kelley, S. E., Briner, J. P., and Young, N. E.: Rapid ice retreat in Disko Bugt supported
 930 by ^{10}Be dating of the last recession of the western Greenland Ice Sheet, *Quat Sci Rev*,
 931 82, 13–22, <https://doi.org/10.1016/j.quascirev.2013.09.018>, 2013.

932 Kelly, M. A. and Lowell, T. V.: Fluctuations of local glaciers in Greenland during latest
 933 Pleistocene and Holocene time, *Quat Sci Rev*, 28, 2088–2106,
 934 <https://doi.org/10.1016/j.quascirev.2008.12.008>, 2009.

935 Kelly, M. A., Lowell, T. V., Hall, B. L., Schaefer, J. M., Finkel, R. C., Goehring, B. M.,
 936 Alley, R. B., and Denton, G. H.: A ^{10}Be chronology of lateglacial and Holocene mountain
 937 glaciation in the Scoresby Sund region, east Greenland: implications for seasonality
 938 during lateglacial time, *Quat Sci Rev*, 27, 2273–2282,
 939 <https://doi.org/10.1016/j.quascirev.2008.08.004>, 2008.

940 Khan, S. A., Colgan, W., Neumann, T. A., van den Broeke, M. R., Brunt, K. M., Noël, B.,
 941 Bamber, J. L., Hassan, J., and Bjørk, A. A.: Accelerating Ice Loss From Peripheral
 942 Glaciers in North Greenland, *Geophys Res Lett*, 49,
 943 <https://doi.org/10.1029/2022GL098915>, 2022.

944 Kienholz, C., Rich, J. L., Arendt, A. A., and Hock, R.: A new method for deriving glacier
 945 centerlines applied to glaciers in Alaska and northwest Canada, *Cryosphere*, 8, 503–519,
 946 <https://doi.org/10.5194/tc-8-503-2014>, 2014.

947 Kingma, D. P. and Ba, J.: Adam: A Method for Stochastic Optimization, 2014.

948 Kjær, K. H., Bjørk, A. A., Kjeldsen, K. K., Hansen, E. S., Andresen, C. S., Siggaard-
 949 Andersen, M. L., Khan, S. A., Søndergaard, A. S., Colgan, W., Schomacker, A.,
 950 Woodroffe, S., Funder, S., Rouillard, A., Jensen, J. F., and Larsen, N. K.: Glacier response
 951 to the Little Ice Age during the Neoglacial cooling in Greenland,
 952 <https://doi.org/10.1016/j.earscirev.2022.103984>, 1 April 2022.

953 Lange, S., Menz, C., Gleixner, S., Cucchi, M., Weedon, G. P., Amici, A., Bellouin, N.,
 954 Müller Schmied, H., Hersbach, H., Buontempo, C., and Cagnazzo, C.: WFDE5 over land
 955 merged with ERA5 over the ocean (W5E5 v2.0), ISIMIP Repository [data set],
 956 <https://doi.org/10.48364/ISIMIP.342217>, 2021.

957 Larocca, L. J., Axford, Y., Bjørk, A. A., Lasher, G. E., and Brooks, J. P.: Local glaciers
 958 record delayed peak Holocene warmth in south Greenland, *Quat Sci Rev*, 241,
 959 <https://doi.org/10.1016/j.quascirev.2020.106421>, 2020.

960 Larocca, L. J., Twining–Ward, M., Axford, Y., Schweinsberg, A. D., Larsen, S. H.,
 961 Westergaard–Nielsen, A., Luetzenburg, G., Briner, J. P., Kjeldsen, K. K., and Bjørk, A.

962 A.: Greenland-wide accelerated retreat of peripheral glaciers in the twenty-first century,
 963 *Nat Clim Chang*, 13, 1324–1328, <https://doi.org/10.1038/s41558-023-01855-6>, 2023.

964 Lasher, G. E. and Axford, Y.: Medieval warmth confirmed at the Norse Eastern Settlement
 965 in Greenland, *Geology*, 47, 267–270, <https://doi.org/10.1130/G45833.1>, 2019.

966 Lecavalier, B. S., Milne, G. A., Simpson, M. J. R., Wake, L., Huybrechts, P., Tarasov, L.,
 967 Kjeldsen, K. K., Funder, S., Long, A. J., Woodroffe, S., Dyke, A. S., and Larsen, N. K.: A
 968 model of Greenland ice sheet deglaciation constrained by observations of relative sea
 969 level and ice extent, *Quat Sci Rev*, 102, 54–84,
 970 <https://doi.org/10.1016/j.quascirev.2014.07.018>, 2014.

971 Leclercq, P. W., Weidick, A., Paul, F., Bolch, T., Citterio, M., and Oerlemans, J.: Brief
 972 communication historical glacier length changes in West Greenland, *Cryosphere*, 6,
 973 1339–1343, <https://doi.org/10.5194/tc-6-1339-2012>, 2012.

974 Leger, T. P. M., Clark, C. D., Huynh, C., Jones, S., Ely, J. C., Bradley, S. L., Diemont, C.,
 975 and Hughes, A. L. C.: A Greenland-wide empirical reconstruction of paleo ice sheet
 976 retreat informed by ice extent markers: PaleoGrIS version 1.0, *Climate of the Past*, 20,
 977 701–755, <https://doi.org/10.5194/cp-20-701-2024>, 2024.

978 Lowell, T. V., Hall, B. L., Kelly, M. A., Bennike, O., Lusas, A. R., Honsaker, W., Smith,
 979 C. A., Levy, L. B., Travis, S., and Denton, G. H.: Late Holocene expansion of Istorvet ice
 980 cap, Liverpool Land, east Greenland, *Quat Sci Rev*, 63, 128–140,
 981 <https://doi.org/10.1016/j.quascirev.2012.11.012>, 2013.

982 Maussion, F., Butenko, A., Champollion, N., Dusch, M., Eis, J., Fourteau, K., Gregor, P.,
 983 Jarosch, A. H., Landmann, J., Oesterle, F., Recinos, B., Rothenpieler, T., Vlug, A., Wild,
 984 C. T., and Marzeion, B.: The Open Global Glacier Model (OGGM) v1.1, *Geosci. Model*
 985 *Dev.*, 12, 909–931, <https://doi.org/10.5194/gmd12-909-2019>, 2019.

986 Marzeion, B., Jarosch, A. H., and Hofer, M.: Past and future sea-level change from the
 987 surface mass balance of glaciers, *The Cryosphere*, 6, 1295–1322,
 988 <https://doi.org/10.5194/tc-6-1295-2012>, 2012.

989

990 Medford, A. K., Hall, B. L., Lowell, T. V., Kelly, M. A., Levy, B., Wilcox, P. S., and
 991 Axford, Y.: Holocene glacial history of Renland Ice Cap, East Greenland, reconstructed
 992 from lake sediments, 2021. Millan, R., Mouginit, J., Rabatel, A., and Morlighem, M.: Ice
 993 velocity and thickness of the world’s glaciers, *Nat Geosci*, 15, 124–129,
 994 <https://doi.org/10.1038/s41561-021-00885-z>, 2022.

995 Miller, G. H., Geirsdóttir, Á., Zhong, Y., Larsen, D. J., Otto-Bliesner, B. L., Holland, M.
 996 M., Bailey, D. A., Refsnider, K. A., Lehman, S. J., Southon, J. R., Anderson, C.,
 997 Björnsson, H., and Thordarson, T.: Abrupt onset of the Little Ice Age triggered by
 998 volcanism and sustained by sea-ice/ocean feedbacks, *Geophys Res Lett*, 39,
 999 <https://doi.org/10.1029/2011GL050168>, 2012.

1000 Miner, K. R., Turetsky, M. R., Malina, E., Bartsch, A., Tamminen, J., McGuire, A. D.,
 1001 Fix, A., Sweeney, C., Elder, C. D., and Miller, C. E.: Permafrost carbon emissions in a
 1002 changing Arctic, <https://doi.org/10.1038/s43017-021-00230-3>, 1 January 2022.

1003 O'Hara, S. L., Briner, J. P., and Kelley, S. E.: A ^{10}Be chronology of early Holocene local
 1004 glacier moraines in central West Greenland, *Boreas*, 46, 655–666,
 1005 <https://doi.org/10.1111/bor.12234>, 2017.

1006 Osman, M. B., Smith, B. E., Trusel, L. D., Das, S. B., McConnell, J. R., Chellman, N.,
 1007 Arienzo, M., and Sodemann, H.: Abrupt Common Era hydroclimate shifts drive west
 1008 Greenland ice cap change, *Nat Geosci*, 14, 756–761, [https://doi.org/10.1038/s41561-021-](https://doi.org/10.1038/s41561-021-00818-w)
 1009 00818-w, 2021.

1010 Pedersen, A. K., Larsen, L. M., Riisager, P., and Dueholm, K. S.: Rates of volcanic
 1011 deposition, facies changes and movements in a dynamic basin: The Nuussuaq Basin, West
 1012 Greenland, around the C27n-C26r transition, *Geol Soc Spec Publ*, 197, 157–181,
 1013 <https://doi.org/10.1144/GSL.SP.2002.197.01.07>, 2002.

1014 Reusche, M. M., Marcott, S. A., Ceperley, E. G., Barth, A. M., Brook, E. J., Mix, A. C.,
 1015 and Caffee, M. W.: Early to Late Holocene Surface Exposure Ages From Two Marine-
 1016 Terminating Outlet Glaciers in Northwest Greenland, *Geophys Res Lett*, 45, 7028–7039,
 1017 <https://doi.org/10.1029/2018GL078266>, 2018.

1018 Rounce, D. R., Hock, R., Maussion, F., Hugonnet, R., Kochtitzky, W., Huss, M., Berthier,
 1019 E., Brinkerhoff, D., Compagno, L., Copland, L., Farinotti, D., Menounos, B., and
 1020 McNabb, R. W.: Global glacier change in the 21st century: Every increase in temperature
 1021 matters, *Science* (80-.), 379, 78–83, <https://doi.org/10.1126/science.abo1324>, 2023.

1022 Saros, J. E., Anderson, N. J., Juggins, S., McGowan, S., Yde, J. C., Telling, J., Bullard, J.
 1023 E., Yallop, M. L., Heathcote, A. J., Burpee, B. T., Fowler, R. A., Barry, C. D., Northington,
 1024 R. M., Osburn, C. L., Pla-Rabes, S., Mernild, S. H., Whiteford, E. J., Grace Andrews, M.,
 1025 Kerby, J. T., and Post, E.: Arctic climate shifts drive rapid ecosystem responses across the
 1026 West Greenland landscape, *Environmental Research Letters*, 14,
 1027 <https://doi.org/10.1088/1748-9326/ab2928>, 2019.

1028 Schuster L, Rounce DR, Maussion F. Glacier projections sensitivity to temperature-index
 1029 model choices and calibration strategies. *Annals of Glaciology*. 2023;64(92):293-308.
 1030 doi:10.1017/aog.2023.57

1031 Schweinsberg, A. D., Briner, J. P., Miller, G. H., Bennike, O., and Thomas, E. K.: Local
 1032 glaciation in West Greenland linked to North Atlantic ocean circulation during the
 1033 Holocene, *Geology*, 45, 195–198, <https://doi.org/10.1130/G38114.1>, 2017.

1034 Schweinsberg, A. D., Briner, J. P., Licciardi, J. M., Bennike, O., Lifton, N. A., Graham,
 1035 B. L., Young, N. E., Schaefer, J. M., and Zimmerman, S. H.: Multiple independent records
 1036 of local glacier variability on Nuussuaq, West Greenland, during the Holocene, *Quat Sci*
 1037 *Rev*, 215, 253–271, <https://doi.org/10.1016/j.quascirev.2019.05.007>, 2019.

- 1038 Simpson, M. J. R., Milne, G. A., Huybrechts, P., and Long, A. J.: Calibrating a
1039 glaciological model of the Greenland ice sheet from the Last Glacial Maximum to
1040 present-day using field observations of relative sea level and ice extent, *Quat Sci Rev*, 28,
1041 1631–1657, <https://doi.org/10.1016/j.quascirev.2009.03.004>, 2009.
- 1042 Solomina, O. N., Bradley, R. S., Jomelli, V., Geirsdottir, A., Kaufman, D. S., Koch, J.,
1043 McKay, N. P., Masiokas, M., Miller, G., Nesje, A., Nicolussi, K., Owen, L. A., Putnam,
1044 A. E., Wanner, H., Wiles, G., and Yang, B.: Glacier fluctuations during the past 2000
1045 years, <https://doi.org/10.1016/j.quascirev.2016.04.008>, 1 October 2016.
- 1046 Søndergaard, A. S., Larsen, N. K., Lecavalier, B. S., Olsen, J., Fitzpatrick, N. P., Kjær, K.
1047 H., and Khan, S. A.: Early Holocene collapse of marine-based ice in northwest Greenland
1048 triggered by atmospheric warming, *Quat Sci Rev*, 239,
1049 <https://doi.org/10.1016/j.quascirev.2020.106360>, 2020.
- 1050 Thornalley, D. J. R., Oppo, D. W., Ortega, P., Robson, J. I., Brierley, C. M., Davis, R.,
1051 Hall, I. R., Moffa-Sanchez, P., Rose, N. L., Spooner, P. T., Yashayaev, I., and Keigwin, L.
1052 D.: Anomalously weak Labrador Sea convection and Atlantic overturning during the past
1053 150 years, *Nature*, 556, 227–230, <https://doi.org/10.1038/s41586-018-0007-4>, 2018.
- 1054 Thrasher, B., Wang, W., Michaelis, A., Melton, F., Lee, T., Nemani, R. NASA global daily
1055 downscaled projections, CMIP6. *Sci. Data* 9. [https://doi.org/10.1038/s41597-022-01393-](https://doi.org/10.1038/s41597-022-01393-4)
1056 4, 2022.
- 1057 Weertman, J.: The Theory of Glacier Sliding, *J. Glaciol.*, 5, 287303, 1964.
- 1058 Weidick, A.: Historical fluctuations of calving glaciers in south and west Greenland,
1059 *Rapp. Groenl. Geol. Unders.*, 161, 73–79. 1994.
- 1060 Weidick, A.: Observations on some Holocene glacier fluctuations in West Greenland,
1061 *Meddelelser om Grønland*, 165, 202pp., 1968.
- 1062 Weidick, A., Bøggild, C. E., and Knudsen, N. T.: Glacier inventory and atlas of West
1063 Greenland, 1992.
- 1064 Weidick, Anker. and Bennike, Ole.: Quaternary glaciation history and glaciology of
1065 Jakobshavn Isbrae and the Disko Bugt region, West Greenland : a review, *Geological*
1066 *Survey of Denmark and Greenland*, 78 pp., 2007.
- 1067 Yde, J. C. and Knudsen, N. T.: 20th-century glacier fluctuations on Disko Island
1068 (Qeqertarsuaq), Greenland, in: *Annals of Glaciology*, 209–214,
1069 <https://doi.org/10.3189/172756407782871558>, 2007.
- 1070 Young, N. E., Schweinsberg, A. D., Briner, J. P., and Schaefer, J. M.: Glacier maxima in
1071 Baffin Bay during the Medieval Warm Period coeval with Norse settlement, *Sci Adv*, 1,
1072 <https://doi.org/10.1126/sciadv.1500806>, 2015.

1073 Yu, L. and Zhong, S.: Changes in sea-surface temperature and atmospheric circulation
 1074 patterns associated with reductions in Arctic sea ice cover in recent decades, *Atmos Chem*
 1075 *Phys*, 18, 14149–14159, <https://doi.org/10.5194/acp-18-14149-2018>, 2018.

1076 Zekollari, H., Huss, M., and Farinotti, D.: Modelling the future evolution of glaciers in
 1077 the European Alps under the EURO-CORDEX RCM ensemble, *The Cryosphere*, 13,
 1078 1125–1146, <https://doi.org/10.5194/tc-13-1125-2019>, 2019.

1079 Zekollari, H., Huss, M., Schuster, L., Maussion, F., Rounce, D. R., Aguayo, R.,
 1080 Champollion, N., Compagno, L., Hugonnet, R., Marzeion, B., Mojtavavi, S., and
 1081 Farinotti, D.: Twenty-first century global glacier evolution under CMIP6 scenarios and
 1082 the role of glacier-specific observations, *The Cryosphere*, 18, 5045–5066,
 1083 <https://doi.org/10.5194/tc-18-5045-2024>, 2024.

1084